Characterization of Novel Adsorbents for the Recovery of Alcohol Biofuels from Aqueous Solutions via Solid-Phase Extraction

by

Thomas Levario

A Thesis Presented in Partial Fulfillment
of the Requirements for the Degree
Master of Science

Approved July 2011 by the
Graduate Supervisory Committee:

David Nielsen, Chair
Mary Laura Lind
Bryan Vogt

ARIZONA STATE UNIVERSITY

August 2011

ABSTRACT

Emergent environmental issues, ever-shrinking petroleum reserves, and rising fossil fuel costs continue to spur interest in the development of sustainable biofuels from renewable feed-stocks. Meanwhile, however, the development and viability of biofuel fermentations remain limited by numerous factors such as feedback inhibition and inefficient and generally energy intensive product recovery processes. To circumvent both feedback inhibition and recovery issues, researchers have turned their attention to incorporating energy efficient separation techniques such as adsorption in *in situ* product recovery (ISPR) approaches. This thesis focused on the characterization of two novel adsorbents for the recovery of alcohol biofuels from model aqueous solutions. First, a hydrophobic silica aerogel was evaluated as a biofuel adsorbent through characterization of equilibrium behavior for conventional second generation biofuels (e.g., ethanol and *n*-butanol). Longer chain and accordingly more hydrophobic alcohols (i.e., *n*-butanol and *2*-pentanol) were more effectively adsorbed than shorter chain alcohols (i.e., ethanol and *i*-propanol), suggesting a mechanism of hydrophobic adsorption. Still, the adsorbed alcohol capacity at biologically relevant conditions were low relative to other 'model' biofuel adsorbents as a result of poor interfacial contact between the aqueous and sorbent. However, sorbent wettability and adsorption is greatly enhanced at high concentrations of alcohol in the aqueous. Consequently, the sorbent exhibits Type IV adsorption isotherms for all biofuels studied, which results from significant multilayer adsorption at elevated alcohol concentrations in the aqueous. Additionally, sorbent wettability significantly affects the dynamic binding efficiency within a packed adsorption column. Second, mesoporous carbons were evaluated as biofuel adsorbents through characterization of equilibrium and kinetic behavior. Variations in synthetic conditions enabled tuning of specific surface area and pore morphology of adsorbents. The adsorbed alcohol capacity

increased with elevated specific surface area of the adsorbents. While their adsorption capacity is comparable to polymeric adsorbents of similar surface area, pore morphology and structure of mesoporous carbons greatly influenced adsorption rates. Multiple cycles of adsorbent regeneration rendered no impact on adsorption equilibrium or kinetics. The high chemical and thermal stability of mesoporous carbons provide potential significant advantages over other commonly examined biofuel adsorbents. Correspondingly, mesoporous carbons should be further studied for biofuel ISPR applications.

DEDICATION

I would like to thank my family and especially my parents for their complete support throughout this process. Without all your support throughout the years I probably never would have been able to attain a Master of Science in chemical engineering and I thank you for that. Dad, I want to thank you for always teaching me if you are going to do something then do it to the best of your abilities. Mom, I want to thank you for always encouraging me to do what I want to do, even after I decided I wanted to be a chemical engineer. Finally, Mark, Jennie and Kaileen, thank you for supporting me in your very unique ways.

ACKNOWLEDGEMENTS

I would like to thank my advisor Dr. David R. Nielsen for his guidance throughout the last few years as I worked toward my Master of Science degree and associated research projects. I really appreciate all of the assistance he provided in guiding me through various points in my academic career such as applying to graduate school and completing my thesis. I would also like to say thanks for all the opportunities he provided me while working in his laboratory, which include the numerous research projects. I would also like to thank Dr. Bryan D. Vogt and Mary Laura Lind for agreeing to serve on my thesis committee.

I would also like to thank Dr. Vogt and Mingzhi Dai as they both were extremely instrumental and helpful in completing the mesoporous carbon project. Without Dr. Vogt and Mingzhi, there would not have been mesoporous carbons for me to study or any of the material synthesis, characterization data, and discussion in Chapter 4 of this thesis. Additionally, I would like to thank you both for helping to educate me in materials and polymer science, neither of which I knew much about prior to working with you.

I would also like to thank my lab and officemates: Shawn, Becky, Wei, Luis, Yuchen, Jake, Matt R., Ploy, Michael, Matt S., Lucas, and Matt C., as they provided a unique environment in which to have fun and more importantly learn. Thank you all for being my friend throughout the last few years. I'll miss all of you and promise to visit when I can.

TABLE OF CONTENTS

Page

Page

Page

LIST OF TABLES

LIST OF FIGURES

Chapter 1

BACKGROUND

1.1 Second Generation Biofuels

Interest in the production of sustainable biofuels from renewable feed-stocks is sparked by the continuing increase in fossil fuel prices, ever-shrinking petroleum reserves, and legislative as well as environmental concerns. In 2009, liquid transportation fuels accounted for ~29% of the total U.S. energy demand, making the transportation sector the second largest energy consuming sector in addition to being the fastest growing (EIA, 2010). This sizable energy demand (~27 quadrillion BTU) is primarily met through the consumption of nonrenewable and unsustainable petroleum and natural gas resources; the majority of which, ~70%, are derived from foreign sources. Biomass-derived fuels presently provide only ~10% of the total global energy requirement, and an even smaller percentage, ~3%, of the liquid transportation fuel demand. Despite having set mandates to produce 36 billion gal. of total renewable fuels annually by 2022 (EIA, 2007), total U.S. production (almost exclusively bioethanol) reached just over 6.5 billion gal. in 2007 (Dineen, 2008). Meeting these aggressive productivity targets will require the development of next generation biofuels, as well as novel technologies capable of supporting their sustainable and economical production.

Among conventional liquid biofuels, ethanol remains the most actively pursued molecule as a result of its excellent physicochemical characterization and the technological maturity associated with its fermentative production. Ethanol, however, is not an ideal fuel due to its high water solubility and low energy density (Table 1.1), which, as a result, diminishes its compatibility with conventional engines and the current fuel distribution infrastructure (Zheng et al., 2009). Alternatively, researchers have turned their attention to producing longer chain, so-called second generation liquid biofuels,

which include, for example, isopropanol, *n*-butanol, *2*-butanol, *n*-pentanol, and *2*-pentanol (Keasling and Chou, 2008; Connor and Liao, 2009). Interest in second generation biofuels is sparked by their favorable physical and thermodynamic properties (e.g., higher energy density and lower water solubility relative to ethanol; Table 1.1). A particular interest in biologically-derived *n*-butanol as a liquid transportation fuel alternative has re-emerged due to the fact that it is a known fermentation product of many *Clostridium* sp. (Keasling and Chou, 2008; Connor and Liao, 2009), and thus benefits from naturally high productivities.

Table 1.1

Physicochemical Properties of Conventional Second Generation Biofuels

Biofuel	Ethanol	*i*-Propanol	*n*-Butanol	*2*-Pentanol
Vapor Pressure (atm) @ 25°C	0.0312	0.0579	0.0109	0.0106
Normal Boiling Point (°C)	78	82	117	119
$LogK_{o/w}$	-0.26	0.07	0.8	1.13
Water Solubility (g/L) @ 20°C	∞	∞	77	45
Energy Density (MJ/L)	22.7	23.9	26.8	28.4

1.2 Challenges Associated with Fermentative Biofuel Production

A critical challenge which continues to limit the development and viability of all biofuel fermentations results from feedback inhibition caused by product toxicity at relatively low concentrations (Bowles and Ellefson, 1985; Jones and Woods, 1986; Ingram, 1990). For example, feedback inhibition limits maximal ethanol production to final titers of below about 210, 120, and 60 g/L (equivalent to 4600, 2600, and 1300 mM) for the ethanologenic microbes *Saccharomyces cerevisiae* (Walker, 1998), *Zymomonas mobilis* (Rogers et al., 1996), and *Escherichia coli* (Yomano et al., 1998), respectively.

The situation is made worse for longer chain alcohols (due to their increasingly high hydrophobicity, as indicated by their $logK_{o/w}$ values in Table 1.1). For instance, *n*-butanol can induce feedback inhibition towards *C. acetobutylicum* at concentrations as high as ~13 g/L (or 175mM) (Jones and Woods, 1986). As a result, conventional biofuel fermentations remain confined to dilute conditions, which constitute ineffectual feeds for downstream product recovery and purification processes (Straathof, 2003).

Inefficient product separation is often found to be the second greatest contributor to economically-unviable and unsustainable bioprocesses (behind only feedstock costs) (Schugerl and Hubbuch, 2005). Conventional ethanol and *n*-butanol separations from fermentation broths are achieved via distillation, albeit at great energy demand and expense. For instance, distillative recovery from dilute aqueous solutions can contribute to ~10% of ethanol's total product cost (Galbe et al., 2007). Meanwhile, the application of distillation for *n*-butanol recovery is made more challenging as a result of its low vapor pressure (~3-fold less than water at 25^{o}C; Table 1.1) which necessitates the use of multi-stage designs to ultimately achieve acceptable product purity (Luyben, 2008). Furthermore, it should be noted that distillation is an inherently ill-suited technology for integration with continuous bioprocesses as a result of the thermal sensitivity displayed by both cells and essential media components (e.g., carbohydrate substrates). Hence, the application of distillation for alcohol biofuel recovery will forever be relegated to solely supporting batch processes and is not a viable option for continuous bioprocessing.

1.3 *In Situ* Product Recovery (ISPR)

Effects of product inhibition can, however, be mitigated through the development of bioreactor systems exploiting *in situ* product recovery (ISPR) (Schugerl, 2000; Ezeji et al., 2004; Kumar and Gayen, 2011). These 'extractive fermentation' techniques both produce and remove desired bioproducts simultaneously such that inhibitory

concentrations are never realized within the bioreactor. An illustration depicting the principle of ISPR can be found in Figure 1.1. Due to their considerable potential for improving microbial production of biofuels and biochemicals, ISPR approaches such as adsorption (Nielsen and Prather, 2009; Oudshoorn et al., 2009; Silvestre-Albero et al., 2009; Nielsen et al., 2010; Saravanan et al., 2010), gas stripping (Ezeji et al., 2004; Inokuma et al., 2010), pervaporation (Huang et al., 2009; Ma et al., 2009), perstraction (Papadopoulos and Sirkar, 1993), liquid-liquid extraction (Simoni et al., 2010), and membrane extraction (Isono and Nakajima, 1999) have received significant research interest within the last 25 years. However, experts are presently at odds regarding which approach is most effective and efficient. An ideal separation technique should possess characteristics such as high selectivity and removal rate of desired products. Additionally, for ISPR applications, said technique should also be innocuous to fermenting microbes as well as the fermentation broth, demand minimal material and/or energy resources, and display long term performance and stability (Garcia et al., 2011).

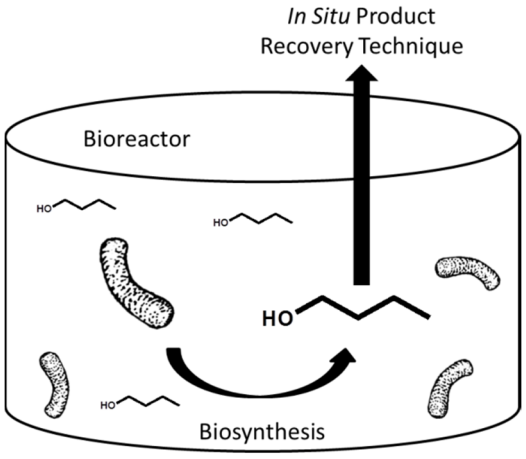

Figure 1.1. Illustrative representation of the general ISPR principle.

Among the aforementioned ISPR approaches, pervaporation, gas stripping, and adsorption tend to be the most actively investigated technologies for biofuel separations due to a variety of factors including their relatively low energy requirements (Ezeji et al.,

2004; Qureshi et al., 2005; Oudshoorn et al., 2009; Kumar and Gayen, 2011). Pervaporation represents a combination of the processes of membrane permeation and evaporation. During pervaporation, a liquid feed side contacts an organic or porous inorganic membrane (Garcia et al., 2011). Target compounds, such as an alcohol biofuel, are then separated from the bulk through adsorption onto the hydrophobic membrane followed by diffusion through to the permeate side. Membranes that have been previously characterized for biofuel separations include, for example, zeolytic and organic polymer membranes (Garcia et al., 2011). Once through to the permeate side, the target molecule is evaporated and recovered through application of vacuum or passing of a sweep gas across the membrane. Figure 1.2 illustrates the process of pervaporation. However, pervaporation presently suffers from low selectivity at high flux or low flux at high selectivity. Furthermore, pervaporation is complicated by membrane fouling caused by other non-biofuel metabolites present in fermentation broths (e.g., salts and sugars) (Garcia et al., 2011), limiting its effective application in ISPR designs.

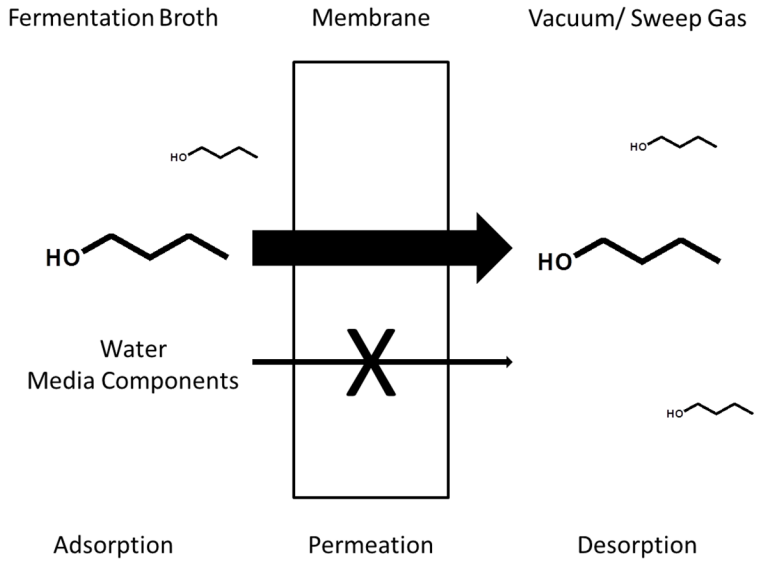

Figure 1.2. Schematic diagram of membrane pervaporation.

Gas stripping is a simple approach for the recovery of volatile biochemical, such as alcohol biofuels, wherein a 'stripping' gas (typically nitrogen or a mixture of fermentation gases; i.e., carbon dioxide and hydrogen) is bubbled through the fermentation broth where it then selectively absorbs desired compounds. Similar to pervaporation, gas stripping involves the transport of target molecules from a bulk liquid phase to an auxiliary gas phase; yet gas stripping is simplified as it does not employ a membrane to separate the two phases. The absence of the membrane provides gas stripping with a significant advantage over pervaporation as there is now no risk of clogging or fouling of the gas phase (Oudshoorn et al., 2009). After the desired products are removed in the stripping gas, they are subsequently collected in a condenser after which the auxiliary phase can then be recycled back into the fermenter for further product removal. Figure 1.3 depicts the process of gas stripping. However, gas stripping also suffers from low selectivity for second generation biofuels, which when applied to the recovery of *n*-butanol has been shown to reach selectivities of approximately 10-14 (Ezeji et al., 2003), 10.3-22.1 (Ezeji et al., 2004), and 4 (Groot et al., 1989) for batch, fed-batch, and continuous fermentation conditions, respectively, thereby limiting its applicability in ISPR approaches for the recovery of biofuels.

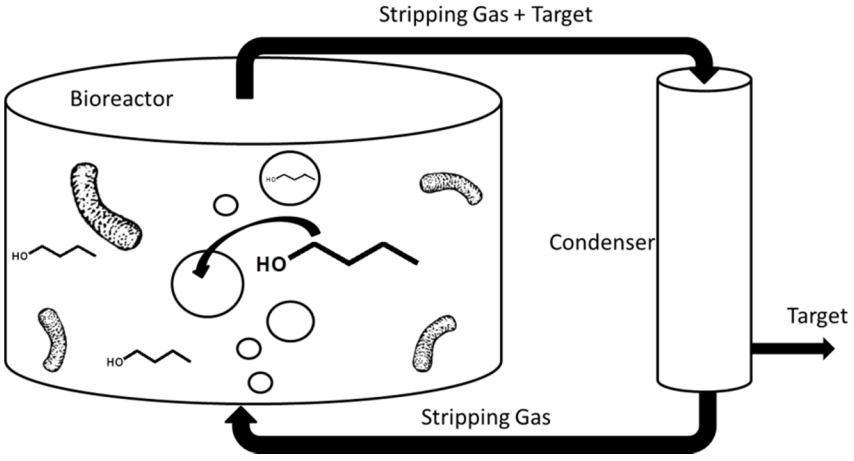

Figure 1.3. Schematic diagram of gas stripping in ISPR.

Adsorption significantly differs from that of pervaporation and gas stripping, wherein target molecules are separated from fluids through their adsorption onto a solid auxiliary phase, so-called solid-phase extraction (SPE). Adsorption of alcohol biofuels from aqueous media proceeds through the development of hydrophobic interactions (i.e., Van der Waals forces) between the surface of the sorbent matrix and alkyl chain of the alcohol (Carey and Sundberg, 2000) as these chemicals physicochemical properties provide no other mechanism for adsorption such as ion-exchange. After adsorption, thermal or pressure swing regeneration can be applied to the recovered adsorbents to release the adsorbate molecules through their vaporization from the adsorbent surface. Figure 1.4 illustrates how adsorption can be integrated with a fermentation for product recovery.

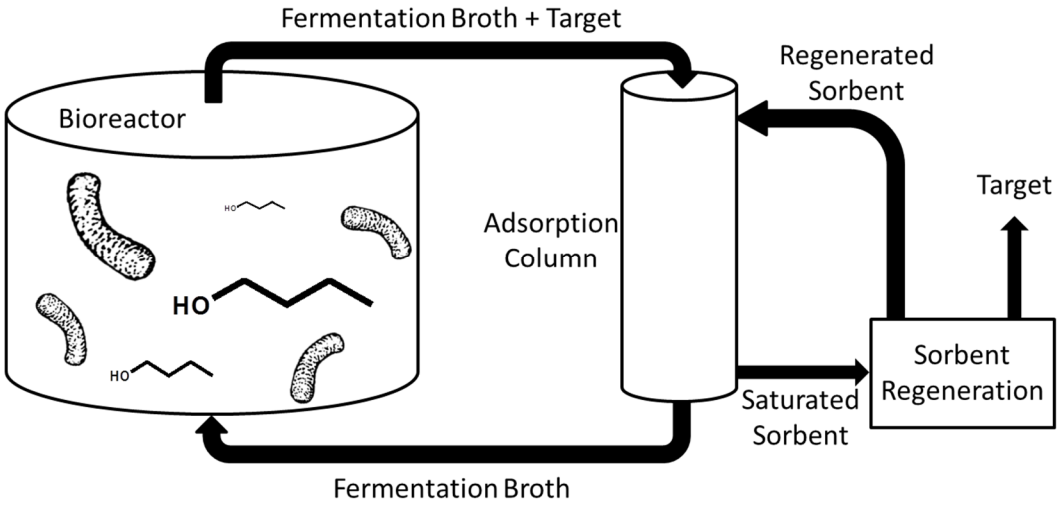

Figure 1.4. Schematic diagram of adsorption in ISPR.

Whereas gas stripping and pervaporation fall short, SPE has been shown to be a promising recovery technique of lower alcohols due to its typically high selectivity (for example, 130-630 for zeolytic adsorbents) as well as high capacity, even at feed concentrations as low as 1 g/L (or 13 mM) *n*-butanol (Oudshoorn et al., 2009), for example. As previously stated, pervaporation, gas stripping, and adsorption are of

particular interest in ISPR applications due to lower associated energy requirements. However, two separate studies which compared the energy efficiency of *n*-butanol ISPR by employing various candidate separation technologies (including distillation, extraction/perstraction, gas stripping, pervaporation, and adsorption), each concluded that adsorption was the most energy efficient approach, providing at least a 10% decrease in the energy requirement of the system (Qureshi et al., 2005; Oudshoorn et al., 2009). Accordingly, adsorption is often considered to possess the highest potential of all ISPR methods, and may play an important role in bridging the economic gap that presently exists between biofuels and petroleum fuels.

1.4 Adsorption as an ISPR Approach

As an alternative approach to conventional biofuel separation processes (e.g., distillation), several researchers have recently turned their attention to the use of adsorption as a means of selectively separating biofuel compounds from dilute aqueous fermentation broths (Ezeji et al., 2004; Oudshoorn et al., 2009; Garcia et al., 2011; Kumar and Gayen, 2011). Numerous different classes of hydrophobic sorbents have previously been studied and characterized for biofuel recovery potential while the most actively investigated include: 1) synthetic polymer resins (Groot and Luyben, 1986; Nielsen et al., 1988; Nielsen and Prather, 2009; Nielsen et al., 2010), 2) inorganic materials (e.g., zeolites) (Milestone and Bibby, 1981; Maddox, 1982; Adnadevic et al., 2008; Oudshoorn et al., 2009; Hashi et al., 2010; Saravanan et al., 2010), and 3) carbonaceous materials (e.g., activated carbons) (Groot and Luyben, 1986; Silvestre-Albero et al., 2009; Hashi et al., 2010). Recent progress regarding the use of materials from each of these three distinct classes will now be individually discussed in further detail. Relevant considerations and commonalities found for all biofuel adsorbents as well as shortcomings will be discussed in more detail in subsequent sections.

1.4.1 Recent work.

1.4.1.1 Inorganic adsorbents. Inorganic materials, principally zeolites and zeolite-analogues, are known for their high selectivity and capacity for hydrophobic solutes as well as their highly-ordered pore structure and thermal stability, thus making them of considerable interest for alcohol biofuel adsorption. One of the earliest studies utilizing such materials as adsorbents for *in situ* product recovery, by Milestone and Bibby (1981), showed that Silicalite (an Al-free zeolite-analogue) can selectively adsorb lower alcohols including methanol, ethanol, *n*-propanol, *n*-butanol, and *n*-pentanol, and found that the loading capacity of said alcohols was improved as the length of the carbon chain increased. Silicalite adsorbed *n*-butanol to a specific loading capacity of approximately 100 mg/g (or 1300 mmol/kg) at model aqueous concentrations of 20 g/L (or 270 mM) (Milestone and Bibby, 1981). Furthermore, in the presence of model aqueous mixtures, Silicalite was found capable of adsorbing *n*-butanol selectively over ethanol, suggesting that Silicalite could potentially be effectively used to separate both compounds in an acetone-butanol-ethanol (ABE) fermentation broth (Milestone and Bibby, 1981). A year later, Maddox (1982) published a study on the use of Silicalite for the recovery of *n*-butanol from actual fermentation broths (as opposed to model solutions used by Milestone and Bibby (1981)), confirming the potential applicability of Silicalite for ISPR of *n*-butanol from fermentation broths. More recently, the adsorption of multicomponent mixtures representing ABE fermentation broths using various zeolites was investigated where it was found that competitive adsorption between adsorbates correlated with their hydrophobicity and that the adsorption affinity decreased from *n*-butanol to acetone to ethanol (Oudshoorn et al., 2009). Additionally, zeolite CBV28014

was capable of adsorbing *n*-butanol as well as acetone at increasingly high capacities (similar to that of Silicalite), and more specifically possessed maximum adsorption capacities (as predicted by the Langmuir adsorption isotherm model) of 118 and 121 mg/g (equivalent to 2000 and 1600 mmol/kg), respectively. Most recently, Saravanan et al. (2010) investigated the adsorption kinetics of *n*-butanol with CBV28014 through various methods including, for example, batch adsorption and frontal analysis in a packed bed. A significant finding from this study is that the batch adsorption of *n*-butanol is strongly influenced by sorbent diameter indicating that the rate of uptake was controlled by pore diffusion of *n*-butanol (Saravanan et al., 2010). As indicated above, inorganic adsorbents such as zeolites possess high selectivity and capacity for alcohol biofuels making them good candidates for *n*-butanol ISPR via adsorption.

1.4.1.2 Polymeric resin adsorbents. The use of polymeric resin adsorbents as a means to separate and recover secondary metabolites (e.g., biofuels) from fermentation broths has been extensively studied. Recent works have demonstrated that polymer adsorbents can provide numerous advantages over alternative sorbents including, for example, elevated (chemical, physical, and biological) stability and improved biocompatibility (Rehmann et al., 2007). In an early study, Nielsen et al. (1988) applied polymeric resin adsorbents for the recovery of acetone and *n*-butanol from ABE fermentations. They found that the addition of the polymeric resin Bonopore (a hydrophobic copolymer composed of poly(styrene-*co*-divinylbenzene), or pSDVB) to cultures enhanced cell growth and *n*-butanol productivity as a result of its ability to adsorb synthesized *n*-butanol at a specific loading capacity as high as 74 mg/g (or 1000 mmol/kg) (Nielsen et al., 1988). More recently, Nielsen et al. (2009) conducted an extensive screening of a series of polymer-based adsorbents for *n*-butanol recovery as applied to the ABE fermentation. Upon first evaluating several adsorbents composed of

differing monomer substituents including, for example, pSDVB, poly(ester), and poly(acrylates), Nielsen et al. (2009) found that those adsorbents composed of the most hydrophobic monomer substituents (for example, styrene in pSDVB) demonstrated the highest affinities for *n*-butanol uptake. Of the 20 polymer adsorbents screened in that study, that which displayed the highest affinity (i.e., solid-sorbent/aqueous-phase partitioning) for *n*-butanol adsorption was Dowex™ Optipore™ L-493 (a macroporous pSDVB) which reached specific loading capacities of up to 175 mg/g (or 2400 mmol/kg) at an aqueous *n*-butanol concentration of 20 g/L (or 270 mM) (Nielsen and Prather, 2009). In a follow-up study, the utility of the same polymeric adsorbents was then applied to other second generation biofuels (e.g., ethanol, *n*-propanol, *i*-propanol, *i*-butanol, *2*-methyl-*1*-butanol, *3*-methyl-*1*-butanol, and *n*-pentanol). In that work, Nielsen et al. (2010) presented a direct correlation between the aqueous-resin partitioning coefficient and specific surface area for resins composed of the same monomer substituent (e.g., all pSDVB copolymers). As indicted above, polymeric resin adsorbents, much like inorganic adsorbents, demonstrate high capacities as well as selectivities for alcohol biofuels from aqueous media and consequently hold considerable promise as a viable biofuel adosrbent.

1.4.1.3 Carbonaceous adsorbents. Application of carbonaceous materials such as activated carbons for the removal of alcohol biofuels is of interest for a variety of reasons including, for example, their low material cost, exceptionally high specific surface areas, thermal stability, and tunable textural and chemical properties (Silvestre-Albero et al., 2009). Groot et al. (1986) provided one of the earliest studies that implemented activated carbon sorbents for the selective recovery of *n*-butanol and *i*-propanol from batch fermentations, wherein comparisons were made against that of commercially-available polymeric resin adsorbents. It was found that Norit-ROW 0.8 (an activated carbon adsorbent) adsorbed the highest amount of *n*-butanol and reached a specific loading

capacity of ~250 mg/g (or 3400 mmol/kg) at an aqueous *n*-butanol concentration of ~15 g/L (or 200 mM), over a 250% improvement of the highest adsorbing polymeric adsorbent investigated in that study (Groot and Luyben, 1986). More recently, Silvestre-Alberto et al. (2009) synthesized and studied a series of activated carbons in order to investigate the roles that porous structure and surface functionalities have during ethanol adsorption. The study indicated that micropore volume (which range between 0.33-0.76 cm^3/g) significantly affected ethanol adsorption and that an optimal volume of 0.54 cm^3/g achieved the highest specific loading capacity. This observed dependence was attributed to either: 1) low specific surface areas attained at low activation of the material or 2) the broadening of pore sizes at high activation (Silvestre-Albero et al., 2009); indicating that the lack of control over pore structure severely limits its adsorptive capacity for alcohol biofuels. In another study which again investigated ethanol adsorption by activated carbons (as well as zeolites for comparison), a linear correlation existing between the specific loading capacity and specific surface area was clearly demonstrated (similar to what Nielsen at al. (2009) found for polymeric adsorbents). More specifically, it was found that adsorption capacity increased with increases in surface area for all materials (Hashi et al., 2010) and that all activated carbons showed adsorption potentials higher than that of any zeolite adsorbent investigated in this particular study. As seen above, carbonaceous materials provide exceedingly high capacities for adsorbing alcohol biofuels from aqueous solutions, and provide a facile means of biofuel ISPR.

1.4.2 Issues with conventional biofuel adsorbents. As previously stated, several conventional biofuel adsorbents show good selectivity as well as capacity for alcohol biofuels and provide differing benefits for ISPR applications. Nevertheless, several important issues continue to limit the application of such materials as adsorbents in biofuel recovery applications. For instance, high thermal stability is an essential

characteristic and would be a prerequisite in any industrial process wherein thermal swing would be used for adsorbent regeneration and biofuel recovery. Such an approach was demonstrated to be effective, for example, for recovering *n*-butanol adsorbed on pSDVB resins (Nielsen and Prather, 2009). However, pSDVB possesses a glass transition temperature of only 95^{o}C and a melting point of ~250^{o}C (depending on the degree of crosslinking), whereas the normal boiling point of *n*-butanol is 117^{o}C (Table 1.1). Furthermore, polymeric adsorbents have been shown to suffer from the negative effects of swelling and thermal expansion which can result in, for example, particle fracture and other mechanical failures. Chemical inertness and stability are also essential features of an ideal biofuel adsorbent, ensuring that the nutrients essential to microbial growth (e.g., carbohydrates and salts) are not interfered and that the adsorbent material does not deteriorate as a function of time or reuse. Zeolytic adsorbents, however, have been shown to suffer from slow hydrolysis and degradation in aqueous systems (Cook et al., 1982), which reduces their long term utility in aqueous environments. Taken together, these issues indicate that conventional biofuel adsorbents each show promise for various and differing reasons; however, as of today, not a single adsorbent is capable of meeting every requirement. Consequently, novel materials that display high thermal and chemical stability as well as chemical inertness need to be investigated and characterized for biofuel adsorption, and explored for long term usage.

1.4.3 Salient trends among biofuel adsorbents. As can be deduced from the above discussion, effective biofuel adsorbents share important common attributes, regardless of their distinct chemical compositions. For instance, it has been shown that those materials of increasingly hydrophobic nature display the strongest affinity for alcohol adsorption (Nielsen and Prather, 2009; Oudshoorn et al., 2009; Hashi et al., 2010; Nielsen et al., 2010; Saravanan et al., 2010). To exploit this principle, adsorbent

hydrophobicity has since been increased by, for example, selecting polymers composed of more hydrophobic monomer substituents (Nielsen and Prather, 2009) and by increasing the Si/Al ratio in zeolites (Saravanan et al., 2010). In addition to a highly hydrophobic adsorbent matrix, effective biofuel adsorbents should also possess high specific surface areas so as to provide a greater number of hydrophobic adsorption 'sites' (Hartmann et al., 2005; Nunes et al., 2008; Nielsen and Prather, 2009; Oudshoorn et al., 2009; Nielsen et al., 2010). With these considerations in mind, it was hypothesized that two additional classes of high surface area, hydrophobic materials, namely hydrophobic silica aerogels and mesoporous carbons, may also hold considerable promise in biofuel recovery applications. Additionally, as these materials are known to be relatively inert, they may also provide enhanced thermal and chemical stability relative to conventional biofuel adsorbents. Relevant considerations and recent progress regarding the use of these materials will now be individually discussed in further detail.

1.5 Silica Aerogel Adsorbents

Silica aerogels are sol-gel derived porous materials that are most widely recognized for possessing the lowest density of any known solid (as low as 0.01-0.02 g/cm^3) (Tabata et al., 2010). This feature stems from remarkably high porosity (>90%) (Wagh et al., 2010), and their exceptionally high specific surface areas (>1000 m^2/g) (Reynolds et al., 2001). Although typically hydrophilic in nature due to their Si-OH surface functionality, aerogels can be made hydrophobic by replacing surface hydroxyl groups with hydrolytically stable hydrocarbon moieties, including, for example, methoxy or ethoxy groups (Standeker et al., 2007). The resultant materials possess surface functionalities of $Si\text{-}OCH_3$ and $Si\text{-}OCH_2CH_3$, respectively, and have been found to display increased contact angles with sessile water droplets (~135-155 degrees) (Wagh et al., 2010). Consequently, silica aerogels possess characteristics that identify them as

potentially excellent biofuel adsorbents as they possess remarkably high surface areas and high hydrophobicity. To the best of our knowledge no prior studies have explored the use of hydrophobic aerogels as an adsorbent media for the selective recovery of second generation biofuels from aqueous solutions.

1.5.1 Recent applications. Hydrophobic silica aerogels have previously been applied in adsorption studies that notably include, for example, oil spill cleanup (Reynolds et al., 2001; Reynolds et al., 2001) and the removal of toxic organic contaminants (such as toluene and xylene) from wastewaters (Hrubesh et al., 2001; Standeker et al., 2007; Gorle et al., 2009; Liu et al., 2009). In a recent study, Reynolds et al. (2001) showed that increasing the hydrophobicity (a desired characteristic of biofuel sorbents) of silica aerogels by incorporating R-CF_3 moieties on the sorbent surface significantly improves oil uptake, increasing specific loadings from ~100 to ~16000 mg/g. Hrubesh et al. (2001), employed a hydrophobic silica aerogel for the selective removal of organic contaminants, including ethanol. In that study, the aerogel adsorbent achieved an ethanol specific loading capacity of 460 mg/g (or 9900 mmol/kg) at an aqueous concentration of 1 g/L (or 22 mM). This remains as one of the highest reported values of ethanol adsorption from aqueous solutions for all adsorbent materials (Hrubesh et al., 2001). Accordingly, we hypothesized that hydrophobic aerogels should also hold promise as adsorbents for other, second generation biofuels. To test this hypothesis, Chapter 3 of this thesis will present the first ever investigation of hydrophobic silica aerogels as adsorbents of second generation biofuels.

1.6 Mesoporous Carbon Adsorbents

The past decade has brought about important advancements in the synthesis and development of mesoporous carbons (MPCs) with highly controlled pore structures, allowing them to serve important roles in applications that include, for example,

hydrogen storage, catalysis, and semiconductors (Hartmann et al., 2005; Meng et al., 2006; Zhuang et al., 2009). Mesoporous carbons are a class of carbonaceous materials that are known for their tunable textural and physical properties, as well as their highly-ordered and uniform pore structures. Various pore structures have been explored and demonstrated including, for example, the hexagonal (P6mm) organization of cylindrical mesopores and body-centered cubic (BCC) (Im3m) organization of spherical mesopores (Meng et al., 2006). As a result of their tunable pore morphologies, MPCs in turn also possess tunable specific surface areas which have been reported to achieve as high as 2580 m^2/g (Zhuang et al., 2009), which is much higher than polymeric adsorbents previously characterized for biofuel recovery. In addition to their relevant characteristics that identify them as potential biofuel adsorbents (e.g., high surface area and hydrophobic surface chemistry), MPCs are also known to display ultrahigh thermal stability, having been shown to maintain physical integrity in non-oxidative environments at temperatures of up to 1400^oC and in air at temperatures of up to 325^oC (Meng et al., 2006). The thermally stable nature of MPCs should prove useful in adsorptive biofuel separation processes as adsorbents can routinely be regenerated by thermal swing desorption in industrial applications. Taken together, the unique and attractive physical properties of MPCs translate into their promising potential as effective alcohol biofuel adsorbents. However, to the best of our knowledge, MPCs have never before been specifically developed and investigated as second generation biofuel adsorbents.

1.6.1 Recent applications. In recent years, MPC adsorbents have been investigated in adsorption applications including, for example, the recovery of vitamin E from organic solutions (Hartmann et al., 2005), the recovery of dye compounds from aqueous solutions (Zhuang et al., 2009), and the removal of volatile organic contaminants (VOCs) from aqueous solutions (Saini et al., 2010). When studying the vitamin E

adsorptive recovery, Hartmann et al. (2005) compared the relative efficacy of activated carbon and two mesoporous carbon adsorbents, ultimately finding that adsorption was strongly influenced by the pore volume and pore diameter for all adsorbents. Although an activated carbon had the highest specific surface area of the studied adsorbents, the mesoporous carbons were in fact capable of adsorbing more vitamin E as they possessed greater surface area within their mesopores as opposed to micropores (as indicated by their pore volumes), unlike that of the activated carbon. Consequently, a greater amount of surface area was accessible on the mesoporous carbon adsorbents to the bulky vitamin E molecules. This phenomenon was further substantiated when Zhuang et al. (2009) investigated the adsorption of bulky dye compounds from aqueous solutions. Again, adsorption of these large molecules was improved (relative to that on activated carbon) through the use of mesoporous carbon adsorbents which possessed greater surface area within mesopores, and larger pore volumes and diameters. With these considerations in mind, we postulated that mesoporous carbons should also hold considerable promise in biofuel separations as they display a particularly hydrophobic matrix and high specific surface area. Chapter 4 of this thesis presents the first ever characterization of mesoporous carbons as adsorbents for the recovery conventional and second generation biofuels.

1.7 Research Objectives and Structure of Thesis

As discussed above, there remains a need to discover and characterize new materials which can facilitate the economical separation of alcohol biofuels from aqueous fermentation broths. With that in mind, this thesis presents a fundamental characterization of two materials which show promise as novel biofuel adsorbents, namely hydrophobic silica aerogels and highly-ordered mesoporous carbons.

The specific objectives related to the characterization of hydrophobic silica aerogels include:

1) To study the equilibrium adsorption isotherms of alcohol biofuels with increasing carbon chain length (i.e., ethanol, *i*-propanol, *n*-butanol, and *2*-pentanol).
2) To investigate the *n*-butanol separation efficiency in a packed column design as a function of various relevant operating parameters.

The specific objectives related to the characterization of highly-ordered mesoporous carbons include:

1) To investigate and model the adsorption isotherms of conventional second generation biofuels (i.e., ethanol and *n*-butanol).
2) To characterize and model the relative adsorption kinetics of *n*-butanol by a selection of mesoporous carbons and conventional polymer adsorbents.
3) To investigate the effects that repeated sorbent regeneration has on the adsorption performance of mesoporous carbons.

This thesis consists of four parts, which include individual case studies exploring the potential utility of silica aerogels and mesoporous carbons as alcohol biofuel adsorbents. Chapter 2 presents all analytical as well as experimental methods that are common between each case study. Chapter 3 presents a case study on the application of silica aerogels for alcohol biofuel adsorption. Experimental results and a detailed discussion are presented. Chapter 4 presents a case study on the application of mesoporous carbons for alcohol biofuel adsorption. Experimental results and a detailed discussion are also presented. Finally, Chapter 5 provides an overall summary of the presented works, as well as the net impacts of the findings. Recommendations regarding future research are also provided.

Chapter 2

ANALYTICAL AND EXPERIMENTAL METHODS

2.1 Introduction

Chapter 2 presents both the analytical and experimental methods commonly used to conduct the research that is presented in this thesis. More specific information regarding these methods as well as other methods as it applies to each individual case study is presented in their respective chapters.

2.2 Analytical Methods

2.2.1 High pressure liquid chromatography (HPLC). High pressure liquid chromatography (HPLC; 1100 series, Agilent, Santa Clara, CA) was used to examine aqueous concentrations of various alcohol biofuels. Separation of solutes was achieved on a ZORBAX Eclipse XDB-C18 column (Agilent, Santa Clara, CA) operated at a constant temperature of 50^{o}C. Filtered and degassed deionized water was used as the mobile phase at a constant flow rate of 1.0 mL/min. Analytes were detected using a refractive index detector, and concentrations were determined using external standards (i.e., calibration curves).

2.3 Experimental Approach

2.3.1 Equilibrium adsorption and modeling. Analyzing adsorption equilibrium data of adsorbent-adsorbate pairs is a typical method for evaluating adsorbent uptake capability. Two of the most common methods for presenting/quantifying adsorption equilibria are through constructing equilibrium adsorption isotherms or the use of theoretical equations that model equilibrium adsorption. Equilibrium adsorption isotherms plot the adsorbate (e.g., biofuel) aqueous phase concentration (C_{aq}) against the adsorbate solid-sorbent phase concentration (or the equilibrium specific loading capacity (q)) for a given (constant) temperature. The resultant behavior can be branded as one of

six different types under IUPAC classification of gas physical adsorption (physisorption) (Figure 2.1). The most common is Type I, which can be described by numerous model equations including, for example, Langmuir and Freundlich isotherm models (to be discussed in more detail later). Type II is indicative of monolayer adsorption at low concentrations while significant multilayer adsorption or pore condensation occurs at higher partial pressures (or higher concentrations for liquid phase adsorption). Type III isotherms occur when the adsorbate-adsorbate interactions are stronger than those of the adsorbent-adsorbate. Type IV and V occur with mesoporous materials that show pore condensation and/or significant multilayer adsorption while also displaying a hysteresis loop in the adsorption-desorption processes, while Type VI displays stepwise multilayer adsorption at higher partial pressures (or concentrations) (Keller and Staudt, 2005). For this thesis, isotherm temperatures of interest will be confined to 30-37^{o}C as these temperatures are relevant to common biofuel fermentation culture conditions.

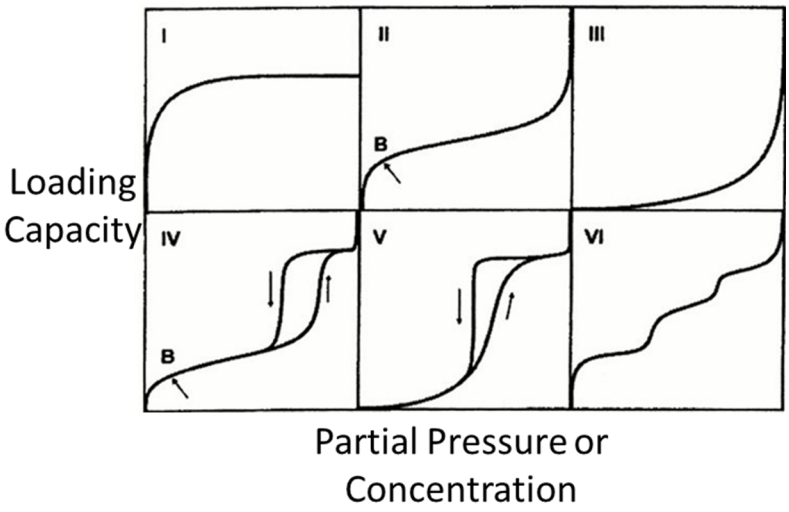

Figure 2.1. IUPAC classification of gas physisorption isotherm types (Keller and Staudt, 2005).

Alternatively, adsorption equilibria can be modeled and predicted by numerous theoretical models, and quite compactly be presented as a group of associated parameters.

Two of the most common equilibrium adsorption isotherm models include the Langmuir and Freundlich equations, which are given as Equations 2.1 and 2.2:

$$q_{eq,\,L} = \frac{q_{eq,max} * k_L * C_{aq}}{1 + k_L * C_{aq}} \tag{2.1}$$

$$q_{eq,\,F} = k_F * C_{aq}^{(1/n)} \tag{2.2}$$

wherein $q_{eq,L}$ and $q_{eq,F}$ are the loading capacities as predicted by the Langmuir and Freundlich equations, respectively, k_L and k_F are the adsorption constants of the Langmuir and Freundlich equations, respectively, $q_{eq,max}$ is the monolayer adsorption or maximum loading capacity, and n is the Freundlich exponent. Although both equations model Type I adsorption behavior, Langmuir was theoretically derived based on the assumption of monolayer adsorption while Freundlich is entirely empirical. For this thesis, equilibrium adsorption data were fit to both models and parameters were estimated via nonlinear least squares regression of the experimental equilibrium data to Equations 2.1 and 2.2 using MATLAB® and the intrinsic function *nlinfit*.

Equilibrium adsorption experiments were set-up by preparing aqueous alcohol solutions in sterile deionized water at initial concentrations relevant to biofuel fermentations. Solutions were then analyzed via HPLC in order to quantitatively determine the initial concentration of biofuel in solution. Adsorbents were then added to the solutions and allowed to equilibrate. After equilibration, the supernatant was removed for HPLC analysis, as described in Section 2.1.1. The specific loading capacity was then determined by the following material balance relationship:

$$q = \frac{C_{aq,o} * V_{aq} - C_{aq} * V_{aq}}{m} \tag{2.3}$$

where $C_{aq,o}$ is the initial concentration of alcohol in the aqueous phase, V_{aq} is the volume of the aqueous phase, and m is the mass of adsorbent. Again, experimental data were subsequently fit to both the Langmuir and Freundlich isotherm models (Equations 2.1

and 2.2). More specific information regarding the set-up of these experiments as it applies to each case study are discussed in further detail in their corresponding chapters.

2.3.2 Dynamic adsorption and modeling. The rate at which adsorption equilibrium is approached (i.e., the adsorption kinetics) is of paramount interest in the design of biofuel production processes. For example, to effectively serve in ISPR applications, biofuel molecules must be adsorbed from the culture medium at rates equal to or greater than their rate of biosynthesis so as to ensure that titers cannot accumulate above relevant inhibitory thresholds. A commonly used method to investigate adsorption kinetics is to analyze the specific loading capacity as a function of time, and model the experimental data with an appropriate equation (much like that of equilibrium adsorption studies). These experiments can be easily set-up as a set of parallel batch adsorption experiments that equilibrate for different amounts of time. If it is assumed that the adsorption process follows pseudo-first order kinetics, then it would be possible to approximate biofuel uptake by the following relationship:

$$\frac{dq}{dt} = k_1 * q_{eq} - k_1 * q_t \tag{2.4}$$

where k_1 is the pseudo-first order kinetic constant, q_{eq} is the equilibrium specific loading capacity, and q_t is the specific loading capacity at time t. Data can be fit to this equation, which would allow predictions to be made about k_1, wherein high values are desired as that indicates fast uptake of solutes.

As specific loading capacities vary between adsorbent-adsorbate pairs, a common method for facilitating comparisons between different materials is through implementation of a normalized scale represented as the fractional saturation (*FS*), which can calculated as:

$$FS = q_t / q_{eq} \tag{2.5}$$

FS values range between 0 and 1, representing no adsorption (the initial condition) and full saturation (the final, equilibrium condition), respectively.

Adsorption kinetics are also characterized through the use of frontal analysis in packed adsorption columns. Packed bed adsorption is one of the most widely used methods in industrial applications for the continuous adsorption of biochemical species from liquid media. Important to these processes is the overall dynamics of the system as it determines the efficiency of the separation, rather than just material-specific equilibrium considerations. The separation efficiency of a packed column is known to be correlated with the dynamic binding capacity of the target solute in the feed solution, and is commonly interpreted by frontal analysis, or breakthrough curves (Yuan and Sun, 2009; Yuan et al., 2010). Breakthrough curves plot concentration of the target solute in the column effluent normalized by the feed concentration as a function of time (or volume of feed supplied). Figure 2.2 illustrates a typical column breakthrough curve.

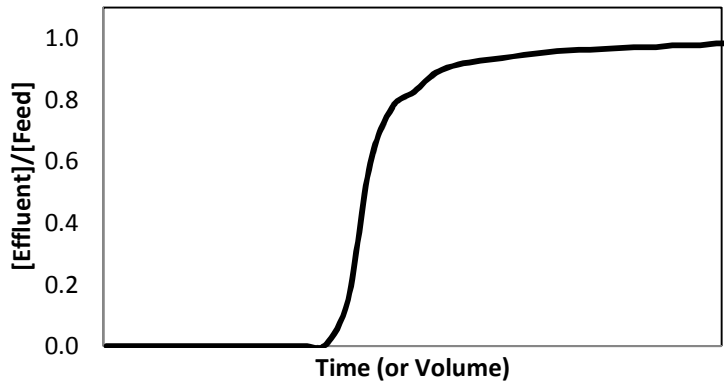

Figure 2.2. Sample breakthrough curve.

Breakthrough curves are useful in that they can be utilized to calculate the dynamic binding capacity as this value is correlated to the area above the curve. If the column is properly designed, the dynamic binding capacity should approach that of the equilibrium loading capacity. However, if significant mass-transfer limitations exist within the

adsorption process, the overall separation efficiency will subsequently suffer as the system would then be controlled by kinetic and not equilibrium processes. More specific data regarding the set-up of these experiments as it applies to each case study are discussed in further detail in corresponding chapters.

Chapter 3

SILICA AEROGEL ADSORBENTS

3.1 Introduction

As mentioned in Chapter 1, implementation of silica aerogels in selective solid-phase extraction could potentially result in the facile separation and recovery of second generation biofuels. This chapter characterizes a commercially available, hydrophobic silica aerogel (Cabot Nanogel TLD302, see Table 3.1 for relevant physical properties) for the liquid phase adsorption of various second generation biofuels, which includes determining the correct isotherm type. As discussed later in this chapter, TLD302 displays an interesting adsorption isotherm that is common among all studied biofuel adsorbates, and an investigation of the possible causes for said isotherm type is presented and discussed in detail. Additionally, this chapter presents the results of applying TLD302 in a continuous *n*-butanol recovery set-up involving a packed bed adsorption column (a commonly used method for the adsorption of solutes in industrial applications).

Table 3.1

Physical Characteristics of Cabot Nanogel TLD302.

Adsorbent	TLD302
Porosity[a]	95% air
Pore diameter[a] (nm)	20-40
Particle diameter[a] (mm)	1.7-2.35
Specific surface area[a] (m^2/g)	~750
Contact angle (degrees)	141.6 ± 2.09
Composition[a]	Silica gel, trimethylsilated

a- As indicated by supplier

3.2 Experimental

3.2.1 Equilibrium adsorption. Equilibrium adsorption experiments were performed in sterile, 17 mL glass Hungate tubes (Bellco Glass, Vineland, NJ) containing 15 mL of aqueous alcohol solution and 250 mg of TLD302. Under these conditions, the entire tube contents were occupied by either solution or aerogel (meaning no headspace volume was present) to promote maximal contact between TLD302 and the aqueous phase. Sealed Hungate tubes were used to facilitate evacuation of the headspace gas by 'bleeding off' (through a needle) as the aerogel-containing tubes were filed with aqueous solution using a needle and syringe. Alcohol solutions were prepared using sterile deionized water at initial concentrations representing the titers that are typical of alcohol fermentations. Equilibrated samples were recovered from the tubes after shaking at 150 rpm for 48 h at 30^{o}C. A temperature of 30^{o}C was selected due to its relevance to many common biofuel fermentation conditions. Alcohol concentrations were measured before and after equilibration in order to determine the specific loading capacity on TLD302 as previously described in Section 2.3.1. The results of these experiments are discussed in detail in Section 3.3.1.

3.2.2 Frontal analysis in a packed bed. Packed bed adsorption column experiments were performed using a glass column (61 cm long x 2.5 cm diameter; Chemglass, Vineland, NJ) filled with 20 g of TLD302. This corresponded to a packed bed height of 50 cm, or 82% of the total column height. Model aqueous *n*-butanol solutions were prepared in filtered deionized water at an initial concentration of either 10 or 55 g/L (equivalent to 135 and 740 mM). The column was oriented vertically and a continuous upward flow was provided by a constant flow pump (LabAlliance Series 1, State College, PA) at rates ranging between 1-10 mL/min. An upward flow was required to attain packed column conditions given the extremely low density of hydrophobic

TLD302 which, regardless of orientation, will float at or near the top of the column, thereby producing an inversely fluidized bed condition if downward flow was applied (an undesired condition for this study). Samples (5 mL) of the column effluent were collected at varying frequency utilizing an Advantec fraction collector (SF-2120, Dublin, CA), and subsequently analyzed by HPLC as previously described in Section 2.2.1. All experiments were performed until complete breakthrough was attained in the column, indicating that equilibrium saturation conditions had been attained in the column. The column was then thoroughly rinsed with deionized water before being recharged with fresh TLD302 and the protocol repeated for different conditions of interest. The results of these experiments are described in Section 3.3.2.

3.3 Results and Discussion

3.3.1 Isotherm determination. In addition to the individual adsorption of naturally-occurring alcohol biofuels ethanol and *n*-butanol, *i*-propanol and *2*-pentanol were also explored in order to more carefully examine the influence of carbon chain length (i.e., 2 through 5). The equilibrium adsorption of ethanol, *i*-propanol, *n*-butanol, and *2*-pentanol by TLD302 across a concentration regime that is relevant to biofuel fermentations are compared in Figure 3.1 together with their respective Freundlich isotherm model predictions. The resultant 'best-fit' model parameter estimates are summarized in Table 3.2.

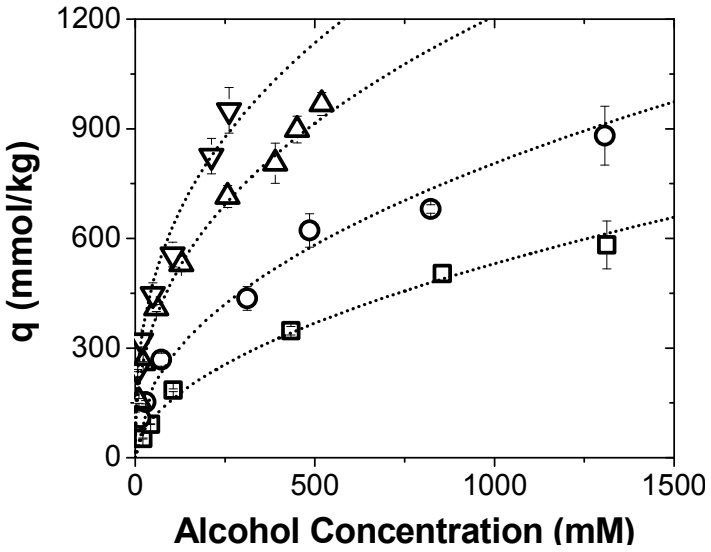

Figure 3.1 Experimental and Freundlich model predictions of ethanol (square), *i*-propanol (circle), *n*-butanol (triangle), and *2*-pentanol (inverted triangle) adsorption equilibria with TLD302.

Table 3.2

Freundlich Adsorption Isotherm Model 'Best-Fit' Parameter Estimates.

Alcohol	k_F (mmol/kg)	*n*
Ethanol	16 ± 9	1.98 ± 0.25
i-Propanol	37 ± 17	2.28 ± 0.32
n-Butanol	70 ± 17	2.39 ± 0.25
2-Pentanol	92 ± 48	2.61 ± 0.61

As expected, both the Freundlich adsorption constant and exponent were found to be positively correlated with the alkyl chain length for each alcohol (i.e., the Freundlich adsorption constant increases as the carbon chain length increases). These same trends have been reported before for hydrophobic polymeric adsorbents that were studied for their ability to adsorb a similar collection of 2-5 carbon biofuel alcohols (Nielsen et al.,

2010). When the adsorption behavior is typified by the Freundlich equilibrium isotherm it is possible to estimate the Gibb's free energy change of adsorption (Δ) as (Huang et al., 2007):

$$\Delta G = -RTn \quad (3.1)$$

where R is the universal gas constant, and T is the temperature of system. The resultant predictions of Gibb's free energy change are compared for each target alcohol in Figure 3.2 wherein a clear negative trend is observed as a function of carbon chain length. These predictions support the hypothesis that more hydrophobic adsorbates are more readily adsorbed by hydrophobic adsorbents such as TLD302 due to the formation of strong surface interactions (e.g., van der Waals forces), and are again consistent with prior works utilizing hydrophobic polymer adsorbents (Nielsen et al., 2010). Furthermore, the predicted values of the Gibb's free energy change of adsorption are consistent with the proposed mechanism of physical adsorption (physisorption) as physisorption interactions, such as Van der Waals forces, are typically lower than ~20 kJ/mol (Kuo et al., 2008).

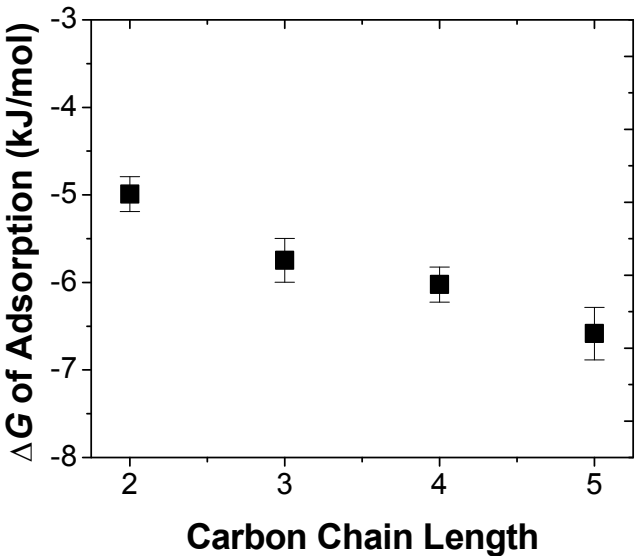

Figure 3.2. Predicted Gibb's free energies of adsorption for alcohols with TLD302 as a function alcohol carbon chain length.

Despite its high specific surface area and hydrophobic surface chemistry, the observed equilibrium adsorption behavior (Figure 3.1) in fact suggests that TLD302 is not a particularly effective adsorbent under concentrations of direct importance to alcohol biofuel fermentations. This is in contrast, for example, to previously characterized adsorbents such as the hydrophobic, macroporous polymer adsorbent Dowex™ Optipore™ L-493 which, at an aqueous phase concentration of *n*-butanol of 10 g/L (or 135 mM), can reach a specific loading capacity of 300 mg/g (or 4060 mmol/kg) (Nielsen et al., 2010). TLD302, on the other hand, only manages about 10% of that performance, reaching a specific loading capacity of 40 mg/g (or 540 mmol/kg). However, for the sake of complete characterization of TLD302, the adsorption isotherms were further extended to alcohol concentrations that are well beyond those of biological relevance. Under such concentrations, it should be noted that the prospects of ISPR would no longer be valid as the equilibrated aqueous alcohol concentrations remain well above their respective inhibitory thresholds. Figure 3.3 compares the adsorption behavior for each of the alcohols of interest on TLD302. Note that in order to maintain a single liquid phase, different aqueous concentrations were used for each alcohol. In all cases, it was found that the equilibrium adsorption followed isotherms that are typified by Type IV behavior, suggesting the occurrence of either 1) significant multilayer adsorption, or 2) penetration into the pores (followed by adsorption) (Keller and Staudt, 2005).

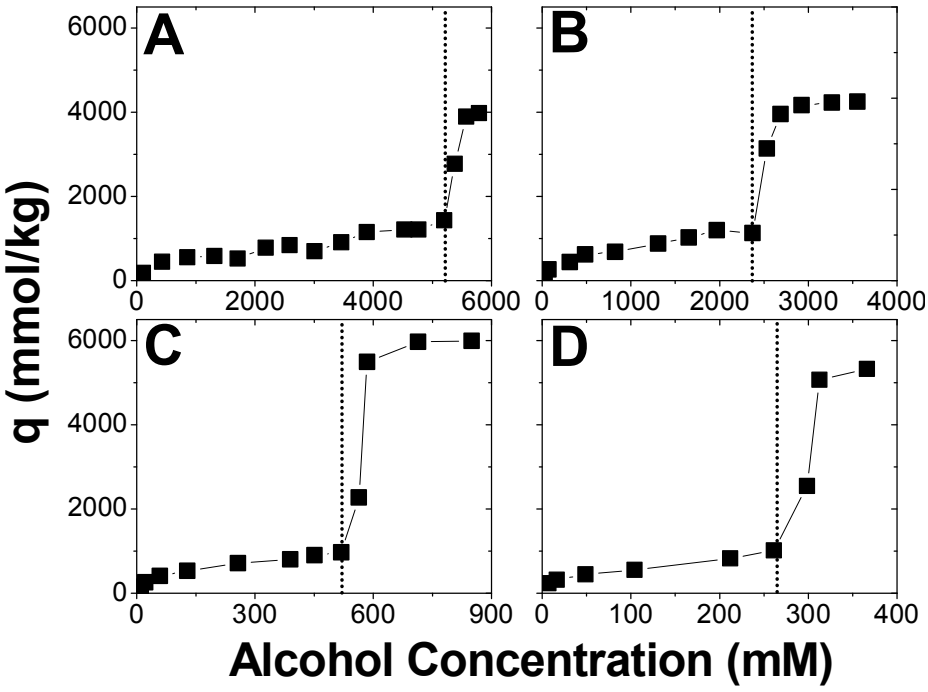

Figure 3.3. Experimental data of ethanol (A), *i*-propanol (B), *n*-butanol (C), and 2-pentanol (D) adsorption equilibria with TLD302. 'Breach point' indicated by a vertical dotted-line.

As can be seen in Figure 3.3, a so-called 'breach point' (i.e., the point or region along the isotherm where a significantly increased rate of change in specific loading capacity is observed as a function of increasing equilibrium alcohol concentration) occurs at a characteristic aqueous concentration for each alcohol, leading to significantly enhanced equilibrium loadings at subsequently higher concentrations. It should be noted that the more hydrophobic the alcohol (i.e., the longer its carbon chain length) the lower the concentration at which the 'breach point' occurs and that all of the 'breach point' loading capacities are similar in magnitude for each alcohol, regardless of their carbon chain length (i.e., between 1100-1400 mmol/kg). A set of experiments investigating the potential reasons for the observed Type IV adsorption isotherm are discussed and presented in the following section.

3.3.1.1 Investigation of type IV isotherm. In addition to distinct changes in isotherm behavior at elevated aqueous concentrations, notable qualitative changes to TLD302 were also observed during alcohol adsorption experiments. For example, at concentrations below the 'breach point', all particles remained opaque and suspended near the top of the aqueous phase. At lower concentrations particles were also found to coalesce together, forming larger, stable agglomerates. As increasing concentrations approached the 'breach point' for each alcohol, however, said agglomerates began to destabilize, returning the mixture to a slurry of individually-dispersed particles. Finally, at equilibrated concentrations above each characteristic 'breach point', all particles became translucent and sank to the bottom of the sample tube. At the same time, the formation of a gaseous head space within each sealed sample tube was also observed. These qualitative observations signify a number of important physiological changes are occurring as a function of position along the equilibrium isotherm. For instance, at increased biofuel loadings the mean particle density increases. This density change is predominantly attributed to the displacement of air from the pores of TLD302. The released air is also responsible for forming the aforementioned head space in the sample tube. In fact, at very high alcohol concentrations (for example, 750 mM *n*-butanol and above) small bubbles could even be seen escaping from individual TLD302 particles as the sample equilibrated. Air displacement from TLD302 suggests that high concentration aqueous alcohol solutions more extensively enter its pores in a process called 'pore intrusion'. More specifically, 'pore intrusion' is referred to here as the complete displacement of air from within the pores, thereby allowing for complete coverage of the sorbent surface. Furthermore, our observations suggest that this phenomenon, together with the equilibrium performance of the adsorbent, displays a strong concentration dependence. These observations led us to postulate that greater specific loadings are

possible at higher alcohol concentrations after the occurrence of 'pore intrusion' which enables a monolayer of adsorbate to form over the entire sorbent surface, followed then by the significant accumulation of adsorption multilayers. This hypothesis and its controlling mechanisms were subsequently examined to provide further mechanistic insight.

Solutions were first examined with respect to both surface tension and contact angle with TLD302 to understand the effects of alcohol concentration on fluid properties and interfacial interactions. The results are shown together in Figure 3.4, where it is first seen that increasing alcohol concentration led to a corresponding decrease in surface tension for all samples (Figure 3.4A). It should be noted that the observed trend for *i*-propanol also agrees well with that of prior works (Vazquez et al., 1995). Declining surface tensions are clearly more sensitive to increasing concentrations for solutes with longer alkyl chains. For example, as seen in Figure 3.4A, only a small increase in concentration brings about a significant decrease in surface tension for *2*-pentanol with its five carbons versus ethanol with only two. A direct correlation was found to exist between the characteristic concentration at which each 'breach point' occurred (approximately 5200, 2400, 520, and 260 mM for ethanol, *i*-propanol, *n*-butanol, and *2*-pentanol, respectively, as in Figure 3.3) and the measured solution surface tension at that condition (between about 31-36 mN/m for each alcohol, as in Figure 3.4A). In addition to impacting surface tension, concentration also simultaneously and significantly affected the characteristic wetting behavior of alcohol solutions on TLD302. More specifically, in Figure 3.4B it can be seen that contact angles decreased at high concentrations, corresponding to a transition from non-wetting to wetting (<90 degrees) surface conditions over the concentration regimes explored. As with surface tension, it was likewise found that this wetting behavior was most sensitive for longer chain alcohols

and that the surface wetting of TLD302 at the characteristic 'breach point' for each alcohol similarly corresponded to a common minimum contact angle, namely ~125 degrees. These observed relationships suggest that 'pore intrusion' into TLD302 is greatly influenced by the surface tension of the solution and wettability of the sorbent. Meaning, more specifically, that surface tension and contact angle must be reduced to below characteristic thresholds before 'pore intrusion' can occur (i.e., total displacement of air from within the sorbent matrix and complete surface coverage), thereby then subsequently enabling multilayer adsorption to occur.

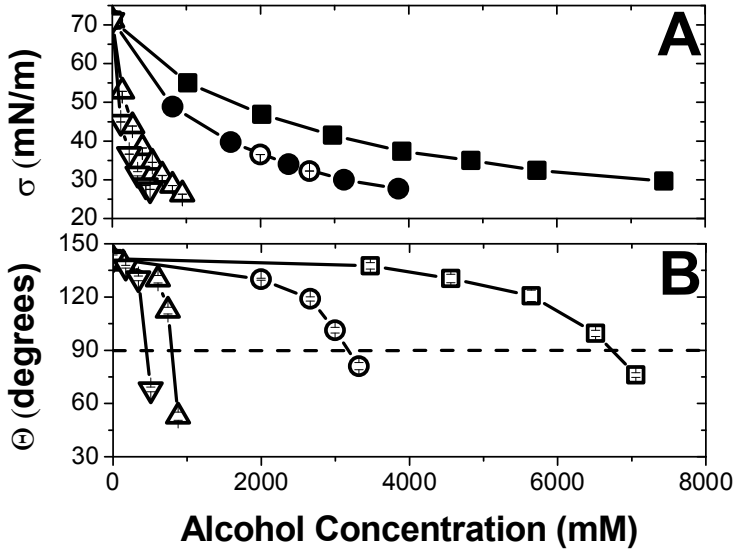

Figure 3.4. (A) Surface tension and (B) sessile droplet contact angle with TLD302 as a function of ethanol (open square, filled square[a]), *i*-propanol (open circle, filled circle[a]), *n*-butanol (open triangle), and *2*-pentanol (open inverted triangle) concentration in aqueous solution. a- (Vazquez et al., 1995).

In addition to affecting 'pore intrusion', surface tension and sorbent wettability appear to play roles in the formation and stability of particle agglomerates. Particle agglomeration has been extensively studied in applications such as gas fluidized bed systems, for example, which incorporate cohesive particles, such as aerogels (McDougall

et al., 2005; Weber et al., 2006; Weber et al., 2008). Multiple mechanisms have been implicated as causing particle agglomeration including, for example, strong interparticle (e.g., Van der Waals) forces (Chaouki et al., 1985) and the presence of binder agents that can act as material bridges (Weber et al., 2008). It has also been found that particle agglomeration can likewise be disrupted through multiple different mechanisms including, for example, application of external mechanical stresses (e.g., increased drag or shear forces), and mass transport of binder substances away from the surface of aggregates which effectively destroy material bridges (Weber et al., 2008). We postulate that a similar mechanism (i.e., mass transport of binder substances) is occurring with TLD302 alcohol adsorption and increasingly high aqueous alcohol concentrations. As a result of the hydrophobic surface chemistry of TLD302, large agglomerates form upon mixing with aqueous solutions to minimize entropic losses associated with interactions occurring between water molecules and the aerogel surface (i.e., Van der Waals forces). In addition, these aggregates are further stabilized by air bridges formed between TLD302 particles. Agglomerate formation reduces the ability of the aqueous solution to displace the air present at the surface of the adsorbent. However, as the aqueous phase alcohol concentration increases, the liquid phase can better contact the solid surface, successfully displace the air, and consequently break down the aerogel agglomerates.

Taken together, these results suggest that as the alcohol solution becomes increasingly hydrophobic (due to either increasing concentrations or by incorporation of longer chain, more hydrophobic alcohols) adsorption by TLD302 is enhanced through multiple, simultaneously occurring mechanisms. First, with decreased surface tension solutions readily destabilize the air bridges formed between individual TLD302 particles, disrupting agglomeration and promoting greater solution-particle contact. Second, improved surface wetting facilitates solution migration into pores whereby air is

subsequently displaced to greatly enhance interfacial contact. As the contact between the aqueous and solid-sorbent phases enhances, the interfacial area wherein alcohols are adsorbed increases, allowing for complete surface coverage and subsequent multilayer adsorption. Correspondingly, the Type IV adsorption isotherm behavior observed herein results from more extensive liquid phase penetration within the pores and resultant surface coverage, followed then by multilayer adsorption.

3.3.2 Frontal analysis in packed bed adsorption. A packed column containing 20 g TLD302 was developed as previously described to evaluate its separation efficiency as a function of a number of relevant operating parameters. The separation efficiency of a packed column is known to be correlated with the dynamic binding capacity of the target solute in the feed solution, and is commonly interpreted by frontal analysis, or breakthrough curves (Yuan and Sun, 2009; Yuan et al., 2010). A feed solution initially containing 10 g/L *n*-butanol (or 135 mM) was first studied to examine separation efficiency and behavior at a maximal concentration that is relevant to fermentation conditions in addition to being below the characteristic 'breach point' of this alcohol at breakthrough (Figure 3.3C). Flow rates of 2.5, 5 and 10 mL/min (equivalent to superficial velocities (u) of 0.5, 1.0, and 2.0 cm/min) were each investigated to determine their effect on the column efficiency, and the resultant breakthrough curves are shown in Figure 3.5. As can be seen, flow rate imposes a significant influence on column breakthrough, as well as efficiency. The breakthrough point was found to be delayed by lowering the flow rate, indicating that a higher dynamic binding capacity was realized before breakthrough occurred. Upon breakthrough, no obvious difference in overall dynamic binding capacity is observed at the two lowest superficial velocities (0.5 and 1.0 cm/min) because, under these conditions, equilibrium conditions are readily attained and control the adsorption. Meanwhile, at a superficial velocity of 2.0 cm/min, the efficiency of the column

diminishes as the dynamic adsorption capacity is no longer controlled by full equilibration, but rather by the adsorption kinetics.

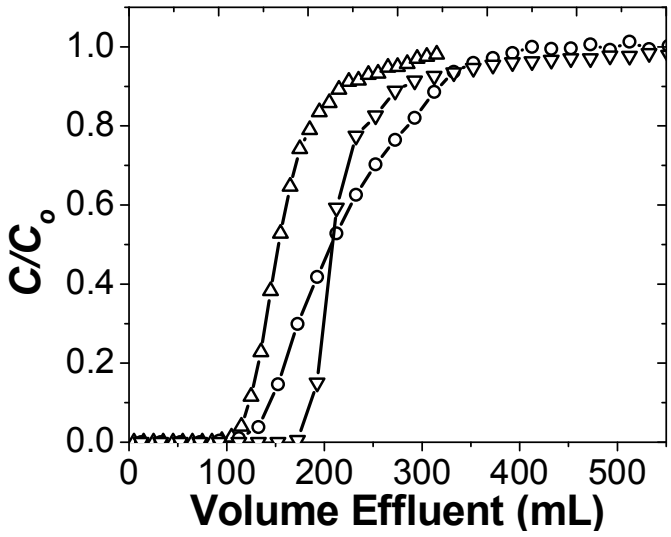

Figure 3.5. *n*-Butanol packed column breakthrough curves with TLD302 at volumetric flow rates of 2.5 (inverted triangle), 5 (circle), and 10 mL/min (triangle) with inlet concentration of 10 g/L.

The height equivalent to a theoretical plate (HETP) is a common parameter used for interpreting the overall chromatographic efficiency of a packed column. In general, steeper slopes of the breakthrough curve correlate with lower HETP values, and thus higher efficiency. In the present study, the lowest superficial velocity (0.5 cm/min) corresponds to the steepest breakthrough curve, indicating that HETP increases with increasing the superficial velocity in the TLD302 column. HETP can be described by van Deemter equation (van Deemter et al., 1956):

$$HETP = \frac{A}{u} + B + Cu \qquad (3.2)$$

where A, B, and C are empirical parameters which capture the unique effects of mass transfer resistance associated with the particular experimental system of interest. Mass transfer resistance in TLD302 columns is predominantly controlled by slow rates of

diffusion into the pores which, as discussed above, is largely influenced by the presence of air within the aerogel which prevents facile 'pore intrusion' (Trzpit et al., 2009), and subsequent adsorption. The rapid and complete breakthrough at a superficial velocity of 2.0 cm/min is not an appropriate operating condition as it can be inferred that the HETP is higher than the packed column height. As seen in Figure 3.5, the dynamic binding capacity did not reach the static equilibrium loading capacity before full breakthrough, wherein the equilibrium area (left of the breakthrough curves) was achieved by both 0.5 and 1 cm/min. That is, the actual packed column height used did not satisfy a single theoretical plate (or equilibrium stage) at high flow rates, because inadequate time was provided for *n*-butanol to diffuse within the sorbent matrix of TLD302.

Next, frontal analysis was performed on the same TLD302 packed columns, however, now employing an *n*-butanol solution of a higher initial concentration (55 mg/L or 740 mM). As seen in Figure 3.3C, breakthrough at such a high initial *n*-butanol concentration will correspond to equilibrated TLD302 particles that exist above the characteristic 'breach point' of this alcohol (Figure 3.3). As seen in Figure 3.6, breakthrough occurs for each flow rate at similar total volumes (between 125-165 mL) of applied solution as did when a lower concentration feedstock was used (Figure 3.5). Interestingly, upon initial breakthrough at the higher feed concentration, for each flow rate it was observed that the effluent was merely ~80% of the feed concentration, which corresponds to approximately 620 mM (just beyond the 'breach point', Figure 3.3C). This sub-maximal effluent concentration was maintained for an additional ~200 to 1200 min (or a total of ~1000 mL of solution) before full breakthrough finally occurred, as seen in Figure 3.6.

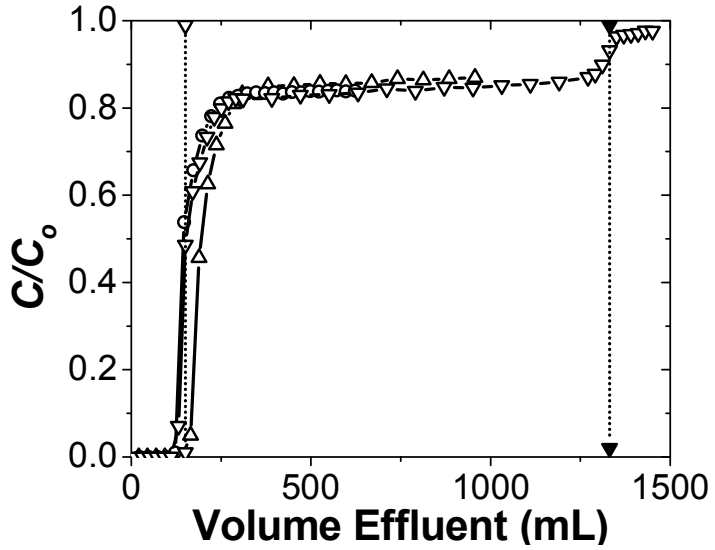

Figure 3.6. n-Butanol packed column breakthrough curves with TLD302 at volumetric flow rates of 1 (inverted triangle), 2.5 (circle), and 6 mL/min (triangle) with inlet concentration of 55 g/L. 'Start of pore intrusion' indicated by vertical-dotted line with open symbols. 'End of pore intrusion' indicated by vertical-dotted line with closed symbols.

Such non-ideal performance of the packed columns resulted from the discontinuous (Type IV) equilibrium behavior of the TLD302 adsorbents and was typified by the apparent segregation of the particles into two distinct yet dynamically interconnected subgroups. More specifically, this included particles equilibrated to specific loadings that existed: 1) below the 'breach point' of the adsorption isotherm, and 2) above the 'breach point' (see Figure 3.3). At the beginning of column breakthrough experiments, all TLD302 particulates were suspended towards the top of the column and were opaque in appearance. However, as the *n*-butanol containing feed continued to be passed up through the column, those TLD302 particles existing at the bottom of the packed bed (i.e., closest to the entrance of the column) were quickly subjected to 'pore intrusion', after which their density increased (due to air evacuation) and they settled

towards the bottom of the column. As the first identifiable aerogel particles visibly experienced pore intrusion (i.e., changed appearance from opaque to translucent and sank to the bottom of the column), the time (or volume of effluent) was noted as the 'start of pore intrusion', as seen in Figure 3.6. As was demonstrated in Figure 3.3, as particles undergo 'pore intrusion' they quickly become more effective *n*-butanol adsorbents (as a result of significant multilayer adsorption), thus rendering the bottom section of the column more efficient than the upper section. As the *n*-butanol concentration profile advances further up through the column, more and more particles (located further up the column) undergo 'pore intrusion', transitioning across the 'breach point' equilibrium to also become more effective *n*-butanol adsorbents. Finally, once all particles had experienced 'pore intrusion', the time (or volume of effluent) was accordingly noted as the 'end of pore intrusion' as seen in Figure 3.6, and corresponds to full breakthrough of the column.

The column efficiencies, however, did not show any difference between the superficial velocities of 0.2 and 1.2 cm/min, which differs from the expected outcome that was observed when a lower feedstock concentration was applied (Figure 3.5). That is, the points at which breakthrough occurred are the same for all three flow rates studied (specifically, ~125 mL for 0.2 and 0.5 cm/min and 160 for 1.2 cm/min). Similar column efficiencies were caused by the increased feedstock concentration, which made the internal mass-transfer resistance no longer important at such an exceedingly high concentration gradient (Fick's law) wherein only large differences in applied flow rates may potentially affect the column efficiency.

Taken together, these packed column results further confirm the concentration dependence of the 'pore intrusion' phenomenon. Additionally, these findings demonstrate that 'pore intrusion' does not instantaneously occur at elevated concentrations, but rather

that a kinetic limitation exists which can impact dynamic processes such as packed beds. This is demonstrated by the observed delay to breakthrough seen in Figure 3.6, and arises from mass-transfer limitations associated with capillary flow such as interfacial friction (Sokhan and Quirke, 2004). Furthermore, as the porous structure of silica aerogels are exceedingly random, properties such as surface roughness (Cottin-Bizonne et al., 2003) and wettability (Sokhan et al., 2001) also play a role on, and in this case potentially inhibit, intraparticle diffusion of adsorbates and removal of air from the pores. Moreover, the point at which 'pore intrusion' was observed to affect every TLD302 particle (i.e., all particles were fully saturated) in Figure 3.6 matches that of full breakthrough. This result produces a mass-transfer region in the breakthrough curve that is dominated by solid-phase diffusion (i.e., diffusion within the pores of TLD302), as is clearly indicated in Figure 3.6 (the region between the dotted-lines for the flow rate of 1 mL/min). This further confirms that adsorption within the pores of TLD302 is controlled by 'pore intrusion' and multilayer adsorption.

3.4 Conclusion

With demonstrated significantly lower specific loading capacity as compared to conventional biofuel adsorbents, the silica aerogel, Cabot Nanogel TLD302, does not possess much potential as a material that can be effectively incorporated in in situ product recovery methods for the separation and purification of lower alcohols via solid-phase extraction. The observed loading capacities were found to be limited at biologically-relevant titers by the inability of the aqueous phase to displace air at the sorbent surface and within the pores, and, therefore, limiting the availability of adsorption 'sites' present at the sorbent surface. However, it was found that at increasingly high concentrations of alcohol in the aqueous phase improved adsorption capacities for all four alcohols investigated as well as producing the observed Type IV adsorption isotherm. The Type

IV adsorption isotherm is a result of improved sorbent wettability at high aqueous alcohol concentrations as the aqueous becomes increasingly hydrophobic in character due to the increasing alcohol content. Accordingly, the application of TLD302 in continuous packed column adsorption of n-butanol displayed rather low dynamic binding capacities in addition to another distinctive phenomenon at elevated *n*-butanol concentrations in the feed (i.e., above that of the 'breach point'). It was observed that complete breakthrough was delayed as a result of mass-transfer limitations associated with pore penetration and subsequent adsorption.

Chapter 4

MESOPOROUS CARBON ADSORBENTS

4.1 Introduction

As mentioned in Chapter 1, implementation of mesoporous carbons in selective solid-phase extraction could potentially result in the facile separation and recovery of second generation biofuels. This chapter presents the synthesis and characterization of four mesoporous carbons. The mesoporous carbons were subsequently characterized for both the equilibrium and dynamic adsorption of two conventional biofuels (i.e., ethanol and *n*-butanol). Dynamic experiments are particularly of interest with regards to mesoporous carbons as they possess tunable physical and textural properties such as pore geometry. Investigating a selection of mesoporous carbons with various pore morphologies may yield important information about how to enhance the adsorption rate, which, as previously discussed in Chapter 1, is extremely vital to ISPR in bioprocesses. Results of these experiments are presented and discussed. Additionally, this chapter explores the thermal and chemical stability of the studied mesoporous carbons by investigating the adsorption performance as well as physical integrity as a function of adsorbent regeneration. Finally, in addition to the four mesoporous carbons studied here, a conventional biofuel adsorbent, Dowex™ Optipore™ L-493, was included in order to facilitate comparisons.

4.2 Experimental

4.2.1 Mesoporous carbon synthesis. The studied mesoporous carbons were synthesized in a collaborating laboratory at Arizona State University (Dr. Bryan D. Vogt, PI and Mingzhi Dai, Ph.D. candidate). Four different mesoporous carbons were synthesized and follow the naming protocol from previous work (Song et al., 2010). A hexagonal organization (*P6mm*) of cylindrical mesopores was obtained by dissolving

resol and Pluronic P123 at molar composition of phenol/ formaldehyde/ NaOH/ F127 = 1: 2: 0.1: 0.012 in ethanol; followed by evaporation of ethanol and producing a polymer film (which was subsequently milled into a fine powder) labeled FDU-15-800 (Meng et al., 2006). A body centered cubic (BCC) organization (*Im3m*) of spherical mesopores was achieved by dissolving resol and Pluronic F127 at molar composition of phenol/ formaldehyde/ NaOH/ F127 = 1: 2: 0.1: 0.006 in ethanol; followed by evaporation of ethanol producing a polymer film (which, again, was subsequently milled into a fine powder) labeled FDU-16-800 (Meng et al., 2006). The phenolic resin in these polymeric powders (FDU-15-800 and FDU-16-800) was then thermally cross-linked at 120 ºC for 24 h. Carbonization was performed in tubular furnace under nitrogen atmosphere with a flow rate of 140 cm^3/min at 800 ºC for 2 h with heating rates of 1 ºC/min below 600 ºC, and 5 ºC/min above 600 ºC In order to increase the surface area of mesoporous carbons, silica through the condensation of TEOS was included in the synthesis solution and followed the procedures listed above. The silica was subsequently removed in 1 M NaOH after carbonization, which produced two different materials labeled as CS-68-800 (Precursor solution: 0.208 g TEOS, 0.1 g resol, and 0.1 g Pluronic F127) and CS-81-800 (Precursor solution: 0.416 g TEOS, 0.1 g resol, and 0.14 g Pluronic F127).

4.2.1.1 Mesoporous carbon characterization. After the mesoporous carbons were synthesized, their full characterization was investigated and the procedures are described here. X-ray diffraction (XRD) in □/2□ geometry with Cu K□ source (PANalytical X'Pert PRO) was used to verify the ordered mesostructures of the four carbons. A parallel plate collimator was used along with an incident beam optical module providing an X-ray beam with very low divergence. The angle of incidence, □, was varied from 0.25 to 1.5 degrees. In order to visualize the mesopores, transmission electron microscopy (TEM) was performed on the carbon powders using a JEOL 2010F

microscope operating at 200 kV. Nitrogen adsorption/desorption isotherms were measured with a Tristar II 3020 Micromeritics instrument at 77 K. Before the measurement, the samples were degassed at 300 ºC for at least 1h. Specific surface areas were subsequently estimated by means of the Brunauer–Emmett–Teller (BET) method in a relative pressure range of P/P0 = 0.05–0.25. The pore size distribution (PSD) and pore volume were calculated from the adsorption branch of the isotherm by using the Barrett–Joyner–Halenda model.

4.2.2 Equilibrium adsorption. Equilibrium adsorption experiments were performed in sterile, 2 mL glass HPLC vials containing 1 mL of aqueous *n*-alcohol solution and 20 mg of carbon powder. Solutions were prepared in sterile deionized water at initial concentrations ranging from 1-120 g/L (or 22-2600 mM) for ethanol and from 1-70 g/L (or 13-944 mM) for *n*-butanol. Samples were equilibrated for 24 h at 37^{o}C while being agitated at 250 rpm. A temperature of 37^{o}C was selected due to its relevance with respect to many important biofuel fermentations. Upon equilibration, the supernatant was removed for HPLC analysis via pipetting through plastic pipet tips packed with DMCS treated glass wool (to eliminate carryover of MPCs). Analysis of these experiments was conducted as previously described in Section 2.3.1.

4.2.3 Dynamic adsorption. Dynamic adsorption experiments were performed for *n*-butanol using the same experimental setup described in Section 4.2.2; however, in this case a fixed initial concentration of 10 g/L (equivalent to 135 mM) was used. Experiments were initiated by addition of 1 mL *n*-butanol solution to 20 mg of MPC. For each MPC of interest, 9 batch adsorption experiments (each representing 9 distinct time points at which to take a sample) were prepared and performed in parallel. This was done to facilitate analysis with minimal disruption due to sampling time while also eliminating complexities due to volume loss. Samples were well-mixed on a Vortex

Genie 2.0 (Scientific Industries; Bohemia, New York) at 250 rpm for up to 24 h. Aqueous samples were taken periodically (as described above), at time intervals ranging between 15 seconds to several hours. Preliminary experiments indicated that the adsorption process was unaffected by changes in the mixing rate (data not shown), which suggests that the mass transport limitation associated with transfer through the bulk solution to the adsorbent surface was not the rate limiting step, allowing emphasis to be placed on solid-phase diffusion. Again, the specific loading capacity was determined as a function of time for each adsorbent according to a material balance (Equation 2.3).

4.2.4 Sorbent regeneration. Thermal regeneration of adsorbents was performed in this experiment in order to investigate the thermal as well as chemical stability of mesoporous carbons. Sorbent regeneration is a vital process as sorbents are routinely regenerated in numerous industrial applications. It is imperative that adsorbents can withstand such treatment and resist various negative effects of regeneration including mechanical failures such as particle fracture. Throughout the course of this study, mesoporous carbon sorbents were routinely regenerated (up to 10 times). Regeneration was achieved utilizing a two-step protocol that consisted of: 1) drying adsorbents at 110^{o}C for 24 h, and 2) heating at 170^{o}C for an additional 24 h to further release any adsorbed species. It should be noted that this is not an ideal protocol for sorbent regeneration; however, it was implemented to ensure that sorbents were completely regenerated so as to be used in subsequent equilibrium and dynamic adsorption experiments.

4.3 Results and Discussion

4.3.1 Adsorbent characterization. The relevant physical characteristics measured for each of mesoporous carbon are summarized in Table 4.1. These materials possess surface areas between ~500 m^2/g and ~1300 m^2/g, which are consistent with prior

reports found in literature (Zhuang et al., 2009). The surface area for CS materials (i.e., CS-68-800 and CS-81-800) is significantly larger than that of FDU materials (i.e., FDU-15-800 and FDU-16-800) due to the presence of a highly microporous network that is generated by the removal of silica that is included in the synthesis of these materials.

Table 4.1

Summary of Adsorbents Investigated.

Adsorbent	A_{BET} (m^2/g)	V_p (cm^3/g)	d_p (nm)	Mesostructure
FDU-15-800	538	0.028	5.0	*P6mm* (cylindrical)
FDU-16-800	671	0.14	5.8	*Im3m* (spherical)
CS-68-800	1287	1.39	8.2	*Im3m* (spherical)
CS-81-800	1307	1.26	7.2	*Im3m* (spherical)
L-493	>1100[a]	1.16[a]	4.6[a]	*not available*

a- As reported by the manufacturer

The pore size distribution, as determined by B.E.T. N_2 sorption, is relatively fine for each material with the average pore size presented in Table 4.1. The diameter for CS-68-800 is the largest due to a decreased contraction of the resol during carbonization as the aforementioned presence of co-continuous silica reinforces the sorbent matrix. However, further increasing the silica concentration (CS-81-800) actually leads to a decrease in the average pore size presumably due to the volume contraction associated with the condensation of the TEOS precursor. To better visualize the well-defined structure of these materials, Figure 4.1 shows TEM micrographs of the studied mesoporous carbons. Ordered monodisperse pores are distinctly visible in the micrographs except for the CS-81-800 (Figure 4.1D). This decrease in the visible order could be a result of the high initial silica included in the sorbent matrix that was subsequently removed, and,

correspondingly, deteriorated the matrix organization. For a control and reference, hydrophobic, macroporous, polymeric (pSDVB) adsorbent Dowex™ Optipore™ L-493 (hereafter referred to as L-493), with physical characteristics listed in Table 4.1, is used as this adsorbent has been well characterized for biofuel separation (Nielsen and Prather, 2009; Nielsen et al., 2010).

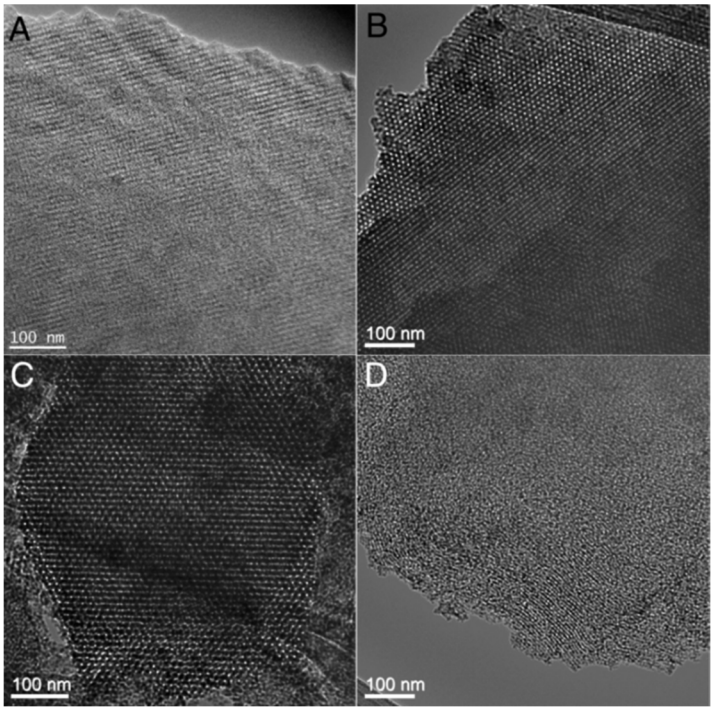

Figure 4.1. TEM images of (A) FDU-15-800, (B) FDU-16-800, (C) CS-68-800, and (D) CS-81-800.

4.3.2 Equilibrium adsorption. Upon comparison with other commonly employed adsorption models (e.g., Langmuir isotherm, Equation 2.1), the Freundlich isotherm model (Equation 2.2) most adequately captures the qualitative behavior of biofuel adsorption by all MPCs studied as a function of concentration (results not shown). Therefore, all equilibrium adsorption data were fit to the Freundlich isotherm model, whose predictions are compared with data in Figure 4.2.

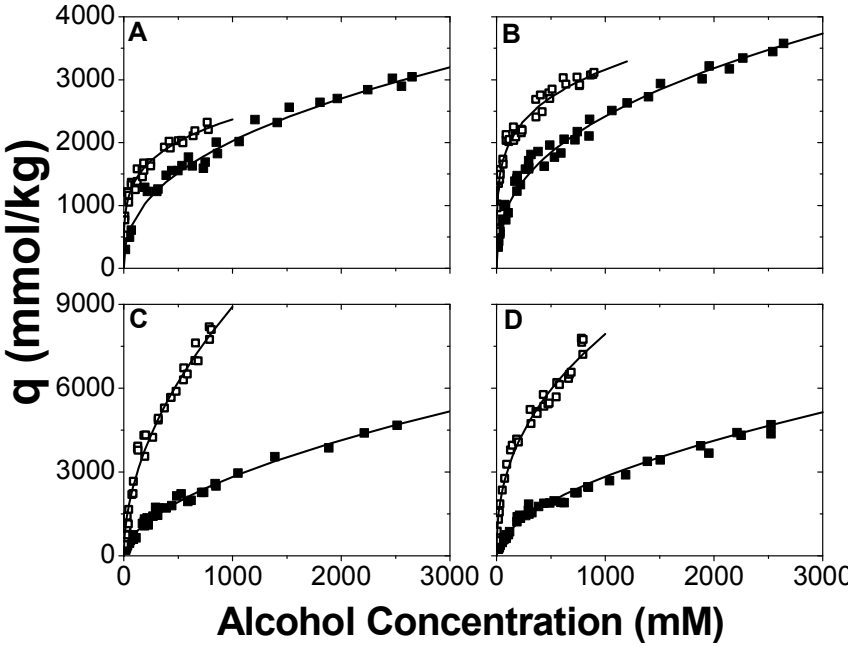

Figure 4.2. Experimental and Freundlich model predictions of ethanol (closed symbols) and *n*-butanol (open symbols) adsorption equilibria with (A) FDU-15-800, (B) FDU-16-800, (C) CS-68-800, and (D) CS-81-800.

Meanwhile, the corresponding parameter estimates are provided in Table 4.2.

Table 4.2

Freundlich Adsorption Model 'Best-Fit' Parameter Estimates.

	Ethanol		*n*-Butanol	
Adsorbent	k_F (mmol/kg)	*n*	k_F (mmol/kg)	*n*
FDU-15-800	115 ± 32	2.41 ± 0.23	371 ± 86	3.65 ± 0.49
FDU-16-800	158 ± 28	2.53 ± 0.16	708 ± 66	4.61 ± 0.34
CS-68-800	62.9 ± 9.4	1.82 ± 0.07	245 ± 59	1.92 ± 0.14
CS-81-800	69.7 ± 10	1.88 ± 0.07	446 ± 95	2.39 ± 0.19
L-493	23 ± 12 [a]	1.25 ± 0.29 [a]	446 ± 115 [a]	2.22 ± 0.26 [a]

a-(Nielsen et al., 2010)

As is consistent with prior studies which have similarly explored the use of hydrophobic adsorbents for biofuel recovery (Nielsen et al., 2010), the adsorption potential (i.e., the magnitude of the adsorbent-aqueous phase partitioning ratio) was observed to increase as the alcohol carbon chain length increased from ethanol (2C) to *n*-butanol (4C). For example, at an aqueous phase concentration of 27 mM (approximately 1 g/L ethanol or 2 g/L *n*-butanol) the adsorbent-aqueous phase partitioning ratio (defined as q_e/C_{aq}) of CS-81-800 increased from 13 (mmol/kg)/(mM) for ethanol to 61 (mmol/kg)/(mM) for *n*-butanol, an improvement of ~470%. As *n*-butanol is greater than 11-times more hydrophobic than ethanol (as predicted by its higher $logK_{O/W}$ value, Table 1.1) its adsorption benefits significantly from larger specific adsorption driving forces (i.e., Van der Waals forces). To verify this statement, the change in Gibb's free energy of adsorption (ΔG) was calculated by Equation 3.1, as previously described in Section 3.3.1. The results of which are summarized in Table 4.3. As expected, the attained values are indicative of physisorption as no value is greater than 20 kJ/mol (Kuo et al., 2008) and the free energy change is greater for *n*-butanol than ethanol for each sorbent, respectively.

Table 4.3

Predicted Gibb's Free Energies of Adsorption for Ethanol and n-Butanol with Each of the Studied Adsorbents.

Adsorbent	ΔG (kJ/mol) Ethanol	ΔG (kJ/mol) *n*-Butanol
FDU-15-800	-6.2	-9.4
FDU-16-800	-6.5	-11.9
CS-68-800	-4.7	-5.0
CS-81-800	-4.8	-6.2
L-493	-3.2	-5.7

The relative magnitudes of k_F and n were also found to be positively correlated with alcohol carbon chain length, a finding which is also consistent with prior studies using polymeric adsorbents such as L-493 (Nielsen and Prather, 2009; Nielsen et al., 2010), whose previously-reported Freundlich isotherm parameters are also listed in Table 4.2. Overall the results presented here demonstrate that the extent of *n*-butanol by MPCs is substantially greater than that which can be achieved with ethanol, a finding which supports the hypothesis that alcohol biofuels are adsorbed by MPCs according to hydrophobic interactions as well as the growing conclusion that alcohol biofuel molecules of increasing carbon chain length (so-called second generation biofuels) show the greatest potential for adsorptive recovery (Ezeji et al., 2004; Ezeji et al., 2004; Nielsen and Prather, 2009; Nielsen et al., 2010). It can also be seen from the *n*-butanol isotherm results of Figure 4.3 that MPC adsorbents can match the adsorption performance of L-493, provided that they are synthesized to possess a comparable specific surface area (Table 4.1). Thus the observed similarities between the adsorption isotherms (as well as the k_F values of Table 4.2) of both CS-68-800 and CS-81-800 and L-493 can be attributed to their similar specific surface areas (Table 4.1). Although the presently-synthesized MPC adsorbents provide no substantial benefits with respect to their achievable extent of biofuel adsorption (relative to L-493), prior works have demonstrated, for example, that MPCs can be synthesized with specific surface areas reaching up to 2580 m^2/g, (~200% greater than CS-81-800) (Zhuang et al., 2009). This significant potential results from the tunable pore morphology of MPCs which should be further exploited for the synthesis of the next generation of hydrophobic biofuel adsorbents.

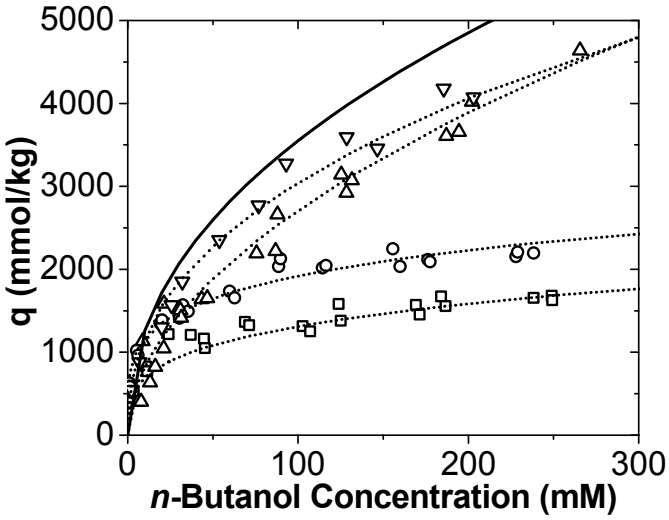

Figure 4.3 Experimental and Freundlich model predictions of *n*-butanol adsorption equilibria with FDU-15-800 (square), FDU-16-800 (circle), CS-68-800 (triangle), and CS-81-800 (inverted triangle). Freundlich model prediction of *n*-butanol adsorption equilibria with Dowex™ Optipore™ L-493 (solid line).

A comparison of Freundlich model parameters, also, indicates noteworthy trends between individual MPC adsorbents. The Freundlich exponent was found to be close in value between each class of MPCs studied (namely between FDU-15-800 and FDU-16-800, and also between CS-68-800 and CS-81-800). Additionally, the relative magnitudes of the Freundlich exponent for both FDU-15-800 and FDU-16-800 (which is an indicator of how sensitive the equilibrium loading capacity is to the equilibrium aqueous phase concentration) are greater than those found for both CS-68-800 and CS-81-800. The high value of k_F for FDU-15-800 and FDU-16-800 results from the high nonlinearity of their adsorption isotherms and is manifested as a sharp bend in the isotherm, which indicates the presence of a pseudo-maximum equilibrium loading capacity (similar to that of the Langmuir adsorption model maximum loading capacity The 'reduced' specific surface area of both FDU-15-800 and FDU-16-800, as compared to CS-68-800 and CS-81 (Table 4.1), limits the maximal amount of alcohol molecules that can be adsorbed on the surface

and, as a consequence, the adsorbents saturate at lower concentrations of alcohol in the aqueous phase. To illustrate this effect, for example, increasing the aqueous *n*-butanol concentration from 67 to 270 mM (equivalent to 5 to 20 g/L) increases the specific loading capacity of FDU-16-800 by ~35% while the specific loading capacity of CS-68-800 increases by ~106% over the same range of equilibrated concentrations. This indicates that the presence of micropores, which significantly increases the specific surface area of MPC adsorbents, improves the equilibrium adsorption by increasing the maximal amount of alcohol that can be adsorbed onto the sorbent surface.

4.3.3 Adsorption kinetics. As *n*-butanol displayed the greatest extent of recovery via hydrophobic adsorption on MPCs, a series of dynamic adsorption experiments were subsequently performed to characterize the kinetics of its adsorption. The results of the dynamic experiments for each of the synthesized MPCs are compared in Figure 4.4, whereas the resultant 'best-fit' estimates of the kinetic constants are listed in Table 4.4.

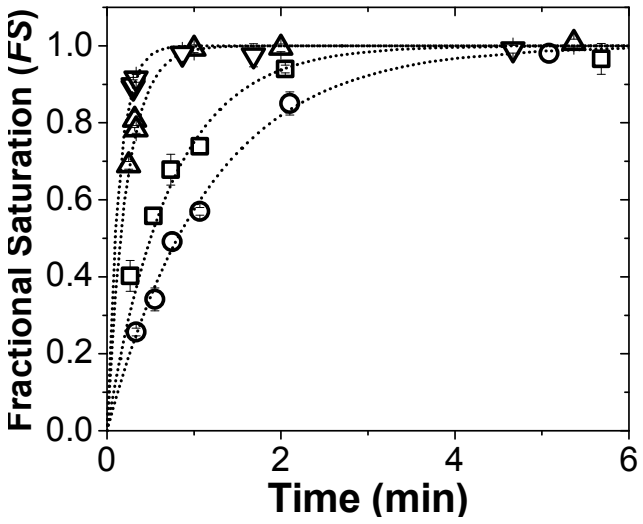

Figure 4.4. Experimental and model predictions of *n*-butanol adsorption dynamics with FDU-15-800 (square), FDU-16-800 (circle), CS-68-800 (triangle), and CS-81-800 (inverted triangle).

As can be seen, the dynamic adsorption associated with each carbon powder is well-described by the proposed, pseudo-first order adsorption model (Equation 2.4). Furthermore, as is illustrated in Figure 4.4, the observed specific rates of adsorption are comparable for each of the synthesized carbon powders, corresponding to the estimated kinetic constants that differ by less than an order of magnitude and are all greater than 0.9 min^{-1} (Table 4.4). These important findings are in stark contrast to the specific *n*-butanol adsorption rates displayed by L-493, a commercially-available, hydrophobic polymer adsorbent which, as discussed above, is a promising adsorbent (as it possesses a high equilibrium affinity for *n*-butanol adsorption) that has been the focus of previous studies on *n*-butanol recovery (Nielsen and Prather, 2009; Nielsen et al., 2010).

Table 4.4

Pseudo-First Order Kinetic Model 'Best-Fit' Parameter Estimates.

Adsorbent	k_1 (min^{-1})
FDU-15-800	1.8 ± 0.43
FDU-16-800	0.9 ± 0.12
CS-68-800	4.5 ± 0.29
CS-81-800	7.5 ± 0.12
L-493	0.05 ± 0.02

Whereas previous characterizations have shown that the equilibrium behavior of L-493 is both qualitatively and quantitatively analogous to that of each of the carbon powders studied here (i.e., the adsorption isotherm behavior and Freundlich model parameters are similar, as compared in Table 4.2), more significant differences are instead observed with respect to the adsorption kinetics. For instance, as can be seen in Figure 4.5, all four MPCs were found to adsorb *n*-butanol more rapidly than L-493, with *n*-butanol adsorbed at specific rates approximately 16-times faster by FDU-16-800 (the slowest adsorbing of

all MPCs studied) than it can be by L-493. From these pseudo-first order kinetic constants it can be predicted, for example, that despite being the slowest adsorbing MPC, FDU-16-800 could reach 99% of its equilibrium specific loading after just 6 min whereas L-493 would require 116 min (nearly 13-times longer) to reach the same extent of equilibration.

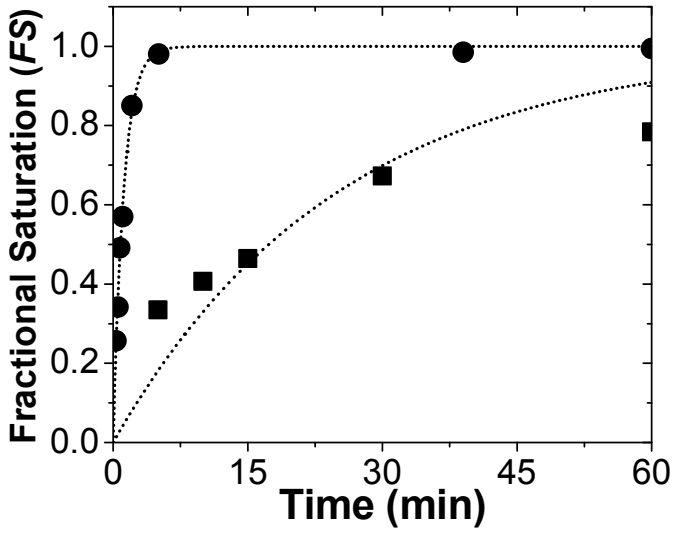

Figure 4.5. Experimental and model predictions of *n*-butanol adsorption dynamics with FDU-16-800 (circle) and Dowex™ Optipore™ L-493 (square).

Whereas each of the MPCs studied demonstrated high specific rates of *n*-butanol adsorption, further consideration of important structural differences between the materials provides an improved mechanistic understanding of the observed behavior. As was presented in Table 4.1, the MPCs examined in this study were of two distinct mesostructures. For instance, despite close similarities in the synthesis protocol used for both FDU-15-800 and FDU-16-800, the two materials differ greatly with regards to their pore geometries and mesostructures. More specifically, FDU-15-800 was synthesized with a hexagonally organized network of cylindrical mesopores whereas FDU-16-800 possesses body-centered cubic (BCC) organized spherical mesopores. As the estimated pseudo-first order kinetic constants for FDU-15-800 and FDU-16-800 were measured to

be two-fold different (1.8 versus 0.9 min^{-1}, respectively) it is proposed that the incorporation of cylindrical mesopores (in comparison to spherical mesopores) more readily facilitates the intraparticle transport of *n*-butanol, improving rates of adsorption and recovery. Meanwhile, whereas each of FDU-16-800, CS-68-800, and CS-81-800 possess the same BCC spherical mesopore structure, both CS-68-800 and CS-81-800 were specifically synthesized so as to be far more perforated by the inclusion of micropores. Not only did this lead to an approximate doubling of surface area and corresponding increase in adsorption equilibria, but this increase in microporosity was also found to have an even more profound effect on adsorption kinetics than even did differences in pore geometry. This led, for example, CS-68-800 and CS-81-800 to have pseudo-first order kinetic constants that were 5.2- to 8.7-times greater (4.5 and 7.5 min^{-1}, respectively) than that of FDU-16-800 (0.9 min^{-1}). There are two potential reasons for the improved kinetics: 1) the highly microporous structure exemplified by CS-68-800 and CS-81-800 might provide a greater number of 'paths' for fluids to enter and leave the adsorbent matrix, and 2) the inclusion of silica during carbonization decreases contraction and produces wider mesopores, which ultimately decreases transport resistance. However, as the pore size decreases from CS-68-800 to CS-81-800 and, still, the kinetic constants do not increase with pore size, we postulate that the former is responsible for the improved kinetics in CS materials. An important consequence of this behavior is that the intraparticle surfaces of the powder are more rapidly wetted by the aqueous medium, a prerequisite for *n*-butanol adsorption across the solid-liquid interface. In contrast, L-493 is a macroporous, poly(styrene-co-divinylbenzene) resin whose random pore structure produces a more tortuous path for intraparticle diffusion (as compared to the highly ordered pore structure of the studied mesoporous carbons) of *n*-butanol before it can access the surface 'sites' for adsorption within the adsorbent matrix. The increased

tortuosity would inversely correlate with a decreased effective diffusion coefficient or pseudo-first order kinetic constant (as it was modeled in the present study), a prediction that is consistent with the observed findings.

Taken together, these results suggest that although the geometry of the mesopores accounts for a marginal influence on the rate of *n*-butanol uptake, the adsorption kinetics are instead more significantly impacted by the microporous structure. Thus, the next generation of carbonaceous biofuel adsorbents should seek to further exploit this feature to enable even greater rates of biofuel adsorption. However, it must also be ensured that the mechanical integrity of the materials should not be compromised as a result; else their utility in actual biofuel processing applications will be diminished.

4.3.4 Sorbent regeneration. Throughout this study we have utilized both virgin and regenerated MPCs for all of the presented adsorption characterization experiments, with no distinguishable differences observed in any case. The use of regenerated adsorbents provides a more accurate representation of an industrial application wherein multiple cycles of adsorption/desorption would be performed on the same adsorbents to minimize capital costs associated with expensive materials. To further confirm that the MPC adsorbents did not suffer from any loss of mechanical integrity or adsorption performance as a result of regeneration and reuse, the nitrogen adsorption/desorption isotherms of both virgin and regenerated samples of CS-81-800 are compared in Figure 4.6. As one can, the isotherm for that of regenerated material remains indistinguishable from that of fresh material, indicating that there were no changes in the porous structure or pore volume. Therefore, it can be concluded that the MPC adsorbents are stable and do not suffer from any loss of performance or integrity resulting from regeneration and reuse.

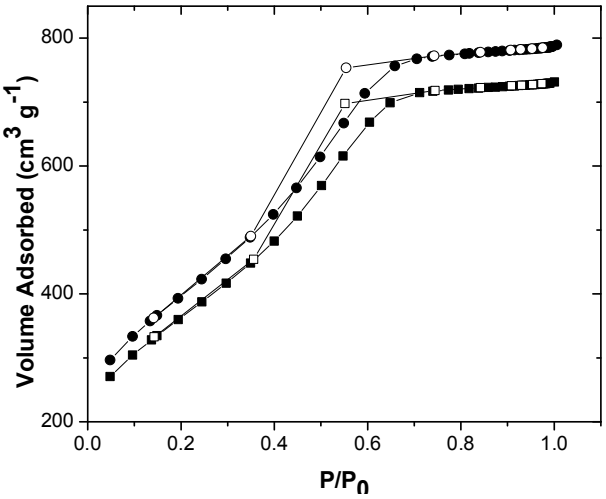

Figure 4.6. B.E.T. N_2 adsorption (closed symbols) and desorption (open symbols) isotherms for CS-81-800 in pristine condition (square) and after multiple separation and regeneration cycles (circle).

Although the adsorbent polymer L-493 was not routinely regenerated and reused within this study, prior works have demonstrated its thermal regeneration in support of repeated *n*-butanol adsorption cycles (Nielsen and Prather, 2009). It should be noted, however, that although pSDVB melts at ~250^{o}C and has a glass transition temperature of ~95^{o}C, the reported upper operating temperature limit for L-493 is reported as 110^{o}C (per manufacturer instructions). In contrast, MPC adsorbents remain stable in a non-oxidative environment at temperatures well beyond 1400^{o}C (Meng et al., 2006), making them ideal for use with thermal cycling in support of biofuel recovery and purification.

4.4 Conclusion

With demonstrated high specific loading capacities and rapid adsorption kinetics, highly-ordered mesoporous carbons possess great potential as biofuel adsorbents. The adsorption kinetics of lower alcohol biofuels upon mesoporous carbons was enhanced through incorporation of highly-ordered and uniform pore structure, and was greatly influenced by both mesopore geometry and by inclusion of micropores. In contrast to

traditional biofuel adsorbents, MPCs possess ultrahigh thermal and chemical stability, greatly promoting their facile regeneration and reuse. No loss of adsorption performance was observed as a result of material regeneration throughout the duration of this study, a promising feature for future industrial applications.

Chapter 5

CONCLUSION

5.1 Summary

Although hydrophobic adsorption holds considerable promise as a viable ISPR approach for the separation and recovery of alcohol biofuels, conventional sorbents do not adequately possess the complement of desired biofuel adsorbent attributes such as high selectivity and capacity, and elevated stability (chemically, thermally, and physically). Thus, new materials must be developed and characterized for biofuel adsorption so as to improve biofuel production efficacy and place biofuels competitively at the economic forefront alongside petroleum based energy resources. This thesis has presented a preliminary characterization of two novel adsorbent materials, namely hydrophobic silica aerogels and highly-ordered mesoporous carbons, as separation media for the recovery of alcohol biofuels from model aqueous solutions.

A hydrophobic silica aerogel (Cabot Nanogel TLD302) was characterized with regards to its biofuel adsorption equilibrium and kinetics. Despite having several desirable attributes of a biofuel adsorbent (e.g., high surface area and hydrophobic surface chemistry), TLD302 was found to display inadequate equilibrium adsorption capacities for alcohol biofuels, relative to previously-characterized biofuel adsorbents. The observed loading capacities were specifically found to be limited at lower aqueous alcohol concentrations as a result of exclusion of aqueous phase from the pores of TLD302 and poor interfacial contact between the liquid and solid phases. At increasingly high alcohol concentrations, however, ‘pore intrusion’ (i.e., the aqueous more readily enters the porous sorbent matrix and completely displaces air from the surface of the sorbent) occurred. This process allowed a monolayer of adsorbate (i.e., alcohol biofuel)

to form on the sorbent surface which was subsequently followed by rapid multilayer adsorption resulting in a unique Type IV adsorption isotherm.

Surfactant templated mesoporous carbons were also evaluated as alcohol biofuel adsorbents through characterization of their equilibrium and kinetic adsorption behavior. Variations in synthetic conditions enabled tuning of specific surface area as well as pore morphology (hexagonally packed cylindrical or BCC spherical pores). It was found that the adsorbed alcohol capacity increased with increases in the specific surface area of adsorbents, regardless of pore morphology. Adsorption capacity was found to be equivalent to that of commercially-available, hydrophobic polymer adsorbents of comparable specific surface areas. Adsorption rates, on the other hand, were greatly influenced by pore morphology and structure, leading to enhancements of up to 1-2 orders of magnitude relative to conventional adsorbents. Mesoporous carbons were routinely regenerated thermally throughout the study and demonstrated no impact on either equilibrium or kinetic behavior.

5.2 Recommendations for Future Work

Based on the presented experimental findings, the following recommendations are suggested for future work on the discovery and characterization of novel biofuel adsorbents:

1. Conduct a more thorough investigation of the 'pore intrusion' phenomenon by incorporating aerogels of differing surface functionality to find if this phenomenon is unique to TLD302 or a common process of highly hydrophobic sorbents. Additionally, utilizing an aerogel of lower hydrophobic character may allow 'pore intrusion' to occur at low enough aqueous alcohol concentrations so that 'pore intrusion' can occur at biologically-relevant titers yielding a high capacity, biofuel adsorbent.

2. Investigate the potential pressure (or temperature) dependence of 'pore intrusion' as increases in pressure may force air out of the sorbent matrix thereby allowing 'pore intrusion' to occur at lower aqueous alcohol concentrations and enhance biofuel adsorption.
3. Synthesize mesoporous carbons of greater surface area than studied here, and characterize biofuel adsorption potential as greater surface area generally correlates to higher adsorption capacities.
4. Fully characterize the thermal, physical, and chemical stability of increasingly high surface area mesoporous carbons to verify without any doubt that these materials a durable for long-term ISPR usage.
5. Perform a more detailed study of the equilibrium and kinetic behavior of mesoporous carbons as a function of regeneration as more regeneration cycles would be desired in industrial applications.
6. Study the efficiency of thermal recovery of biofuels from mesoporous carbons as a function of regeneration temperature and time so that operating conditions can be optimized for ISPR applications.
7. Incorporate mesoporous carbons in continuous recovery applications such as packed column adsorption as continuous production and separation is the desired operation type in industrial applications.
8. Conduct equilibrium and dynamic adsorption studies of mesoporous carbons in actual fermentation broths as it may differ from the reported 'model' adsorption behavior.
9. Investigate competitive adsorption of solutes by mesoporous carbons in applications such as ABE fermentation as MPCs may provide enhanced selectivity of *n*-butanol over acetone and ethanol, in addition to water.

10. Investigate both equilibrium and dynamic adsorption behavior of magnetized mesoporous carbons (e.g., cobalt containing MPCs) for biofuels to facilitate effective MPC separation from aqueous environment.
11. Investigate the effect temperature has on equilibrium adsorption of biofuels by mesoporous carbons as the equilibrium behavior may be further improved as a function of temperature.

REFERENCES

Adnadevic, B., Z. Mojovic and A. Abu Rabi (2008). The kinetics of ethanol adsorption from the aqueous phase onto zeolite NaZSM-5. *Adsorption-Journal of the International Adsorption Society, 14*, 1, 123-131.

Bowles, L. K. and W. L. Ellefson (1985). Effects of butanol on Clostridium acetobutylicum. *Applied and Environmental Microbiology, 50*, 5, 1165-1170.

Carey, F. A. and R. J. Sundberg (2000). *Advanced organic chemistry*. New York; Kluwer Academic/Plenum Pub.

Chaouki, J., C. Chavarie and D. Klvana (1985). Effect of interparticle forces on the hydrodynamic behavior of fluidized aerogels. *Powder Technology, 43*, 2, 117-125.

Connor, M. R. and J. C. Liao (2009). Microbial production of advanced transportation fuels in non-natural hosts. *Current Opinion in Biotechnology, 20*, 3, 307-315.

Cook, T. E., W. A. Cilley, A. C. Savitsky and B. H. Wiers (1982). Zeolite-a hydrolysis and degradation. *Environmental Science & Technology, 16*, 6, 344-350.

Cottin-Bizonne, C., J. L. Barrat, L. Bocquet and E. Charlaix (2003). Low-friction flows of liquid at nanopatterned interfaces. *Nature Materials, 2*, 4, 237-240.

Dineen, B. (2008). Changing the climate: ethanol industry outlook 2008. *Renewable Fuels Association*.

EIA (2007). Energy independence and security act of 2007. Washington, 'Energy Independence and Security Act of 2007', Energy Information Administration, US Department of Energy.

EIA (2010). Annual energy review 2009. Washington, 'Annual Energy Review 2009', US Energy Information Administration.

Ezeji, T. C., N. Qureshi and H. P. Blaschek (2003). Production of acetone, butanol and ethanol by Clostridium beijerinckii BA101 and in situ recovery by gas stripping. *World Journal of Microbiology & Biotechnology, 19*, 6, 595-603.

Ezeji, T. C., N. Qureshi and H. P. Blaschek (2004). Acetone butanol ethanol (ABE) production from concentrated substrate: reduction in substrate inhibition by fed-batch technique and product inhibition by gas stripping. *Applied Microbiology and Biotechnology, 63*, 6, 653-658.

Ezeji, T. C., N. Qureshi and H. P. Blaschek (2004). Butanol fermentation research: upstream and downstream manipulations. *Chemical Record, 4*, 5, 305-314.

Galbe, M., P. Sassner, A. Wingren and G. Zacchi (2007). Process engineering economics of bioethanol production. *Advances in Biochemical Engineering/Biotechnology, 108*, 303-327.

Garcia, V., J. Pakkila, H. Ojamo, E. Muurinen and R. L. Keiski (2011). Challenges in biobutanol production: How to improve the efficiency? *Renewable & Sustainable Energy Reviews, 15*, 2, 964-980.

Gorle, B. S. K., I. Smirnova and M. A. McHugh (2009). Adsorption and thermal release of highly volatile compounds in silica aerogels. *Journal of Supercritical Fluids, 48*, 1, 85-92.

Groot, W. J. and K. C. A. M. Luyben (1986). Insitu product recovery by adsorption in the butanol isopropanol batch fermentation. *Applied Microbiology and Biotechnology, 25*, 1, 29-31.

Groot, W. J., R. G. J. M. Vanderlans and K. C. A. M. Luyben (1989). Batch and continuous butanol fermentations with free-cells - integration with product recovery by gas-stripping. *Applied Microbiology and Biotechnology, 32*, 3, 305-308.

Hartmann, M., A. Vinu and G. Chandrasekar (2005). Adsorption of vitamin E on mesoporous carbon molecular sieves. *Chemistry of Materials, 17*, 4, 829-833.

Hashi, M., F. H. Tezel and J. Thibault (2010). Ethanol Recovery from Fermentation Broth via Carbon Dioxide Stripping and Adsorption. *Energy & Fuels, 24*, 4628-4637.

Hrubesh, L. W., P. R. Coronado and J. H. Satcher (2001). Solvent removal from water with hydrophobic aerogels. *Journal of Non-Crystalline Solids, 285*, 1-3, 328-332.

Huang, H. H., Y. Zhou, K. L. Huang, S. Q. Liu, Q. Luo and M. C. Xu (2007). Adsorption behavior, thermodynamics, and mechanism of phenol on polymeric adsorbents with amide group in cyclohexane. *Journal of Colloid and Interface Science, 316*, 1, 10-18.

Huang, Y. W., J. W. Fu, Y. Pan, X. B. Huang and X. Z. Tang (2009). Pervaporation of ethanol aqueous solution by polyphosphazene membranes: Effect of pendant groups. *Separation and Purification Technology, 66*, 3, 504-509.

Ingram, L. O. (1990). Ethanol Tolerance in Bacteria. *Critical Reviews in Biotechnology, 9*, 4, 305-319.

Inokuma, K., J. C. Liao, M. Okamoto and T. Hanai (2010). Improvement of isopropanol production by metabolically engineered Escherichia coli using gas stripping. *Journal of Bioscience and Bioengineering, 110*, 6, 696-701.

Isono, Y. and M. Nakajima (1999). Application of hydrophobic membrane for alcohol separation from alcohol/aqueous biphase mixture. *Separation and Purification Technology, 17*, 1, 77-82.

Jones, D. T. and D. R. Woods (1986). Acetone-Butanol Fermentation Revisited. *Microbiological Reviews, 50*, 4, 484-524.

Keasling, J. D. and H. Chou (2008). Metabolic engineering delivers next-generation biofuels. *Nature Biotechnology, 26*, 3, 298-299.

Keller, J. and R. Staudt (2005). *Gas Adsorption Equilibria: Experimental Methods and Adsorptive Isotherms*; Springer Science.

Kumar, M. and K. Gayen (2011). Developments in biobutanol production: New insights. *Applied Energy, 88*, 6, 1999-2012.

Kuo, C. Y., C. H. Wu and J. Y. Wu (2008). Adsorption of direct dyes from aqueous solutions by carbon nanotubes: Determination of equilibrium, kinetics and thermodynamics parameters. *Journal of Colloid and Interface Science, 327*, 2, 308-315.

Liu, H. J., W. Sha, A. T. Cooper and M. H. Fan (2009). Preparation and characterization of a novel silica aerogel as adsorbent for toxic organic compounds. *Colloids and Surfaces a-Physicochemical and Engineering Aspects, 347*, 1-3, 38-44.

Luyben, W. L. (2008). Control of the heterogeneous azeotropic n-butanol/water distillation system. *Energy & Fuels, 22*, 6, 4249-4258.

Ma, Y., J. H. Wang and T. Tsuru (2009). Pervaporation of water/ethanol mixtures through microporous silica membranes. *Separation and Purification Technology, 66*, 3, 479-485.

Maddox, I. S. (1982). Use of Silicalite for the Adsorption of Normal-Butanol from Fermentation Liquors. *Biotechnology Letters, 4*, 11, 759-760.

McDougall, S., M. Saberian, C. Briens, F. Berruti and E. Chan (2005). Effect of liquid properties on the agglomerating tendency of a wet gas-solid fluidized bed. *Powder Technology, 149*, 2-3, 61-67.

Meng, Y., D. Gu, F. Q. Zhang, Y. F. Shi, L. Cheng, D. Feng, Z. X. Wu, Z. X. Chen, Y. Wan, A. Stein and D. Y. Zhao (2006). A family of highly ordered mesoporous

polymer resin and carbon structures from organic-organic self-assembly. *Chemistry of Materials, 18*, 18, 4447-4464.

Milestone, N. B. and D. M. Bibby (1981). Concentration of Alcohols by Adsorption on Silicalite. *Journal of Chemical Technology and Biotechnology, 31*, 12, 732-736.

Nielsen, D. R. and K. J. Prather (2009). In situ product recovery of n-butanol using polymeric resins. *Biotechnology and Bioengineering, 102*, 3, 811-821.

Nielsen, D. R., K. L. J. Prather and G. S. Amarasiriwardena (2010). Predicting the adsorption of second generation biofuels by polymeric resins with applications for in situ product recovery (ISPR). *Bioresource Technology, 101*, 8, 2762-2769.

Nielsen, L., M. Larsson, O. Holst and B. Mattiasson (1988). Adsorbents for Extractive Bioconversion Applied to the Acetone-Butanol Fermentation. *Applied Microbiology and Biotechnology, 28*, 4-5, 335-339.

Nunes, C. D., J. Pires, A. P. Carvalho, M. J. Calhorda and P. Ferreira (2008). Synthesis and characterisation of organo-silica hydrophobic clay hetero structures for volatile organic compounds removal. *Microporous and Mesoporous Materials, 111*, 1-3, 612-619.

Oudshoorn, A., L. A. M. van der Wielen and A. J. J. Straathof (2009). Adsorption equilibria of bio-based butanol solutions using zeolite. *Biochemical Engineering Journal, 48*, 1, 99-103.

Oudshoorn, A., L. A. M. van der Wielen and A. J. J. Straathof (2009). Assessment of options for selective 1-butanol recovery from aqueous solution. *Industrial & Engineering Chemistry Research, 48*, 15, 7325-7336.

Papadopoulos, T. and K. K. Sirkar (1993). Separation of a 2-propanol n-heptane mixture by liquid membrane perstraction. *Industrial & Engineering Chemistry Research, 32*, 4, 663-673.

Qureshi, N., S. Hughes, I. S. Maddox and M. A. Cotta (2005). Energy-efficient recovery of butanol from model solutions and fermentation broth by adsorption. *Bioprocess and Biosystems Engineering, 27*, 4, 215-222.

Rehmann, L., B. Sun and A. J. Daugulis (2007). Polymer selection for biphenyl degradation in a solid-liquid two-phase partitioning bioreactor. *Biotechnology Progress, 23*, 4, 814-819.

Reynolds, J. G., P. R. Coronado and L. W. Hrubesh (2001). Hydrophobic aerogels for oil-spill clean up - synthesis and characterization. *Journal of Non-Crystalline Solids, 292*, 1-3, 127-137.

Reynolds, J. G., P. R. Coronado and L. W. Hrubesh (2001). Hydrophobic aerogels for oil-spill cleanup - Intrinsic absorbing properties. *Energy Sources, 23*, 9, 831-843.

Rogers, P. L., K. Lee and D. Tribe (1996). Kinetics of alcohol production by *Zymomonas mobilis* at high sugar concentrations. *Biotechnology Letters, 1*, 165-170.

Saini, V. K., M. Andrade, M. L. Pinto, A. P. Carvalho and J. Pires (2010). How the adsorption properties get changed when going from SBA-15 to its CMK-3 carbon replica. *Separation and Purification Technology, 75*, 3, 366-376.

Saravanan, V., D. A. Waijers, M. Ziari and M. A. Noordermeer (2010). Recovery of 1-butanol from aqueous solutions using zeolite ZSM-5 with a high Si/Al ratio; suitability of a column process for industrial applications. *Biochemical Engineering Journal, 49*, 1, 33-39.

Schugerl, K. (2000). Integrated processing of biotechnology products. *Biotechnology Advances, 18*, 7, 581-599.

Schugerl, K. and J. Hubbuch (2005). Integrated bioprocesses. *Current Opinion in Microbiology, 8*, 3, 294-300.

Silvestre-Albero, J., A. Silvestre-Albero, A. Sepulveda-Escribano and F. Rodriguez-Reinoso (2009). Ethanol removal using activated carbon: effect of porous structure and surface chemistry. *Microporous and Mesoporous Materials, 120*, 1-2, 62-68.

Simoni, L. D., A. Chapeaux, J. F. Brennecke and M. A. Stadtherr (2010). Extraction of biofuels and biofeedstocks from aqueous solutions using ionic liquids. *Computers & Chemical Engineering, 34*, 9, 1406-1412.

Sokhan, V. P., D. Nicholson and N. Quirke (2001). Fluid flow in nanopores: An examination of hydrodynamic boundary conditions. *Journal of Chemical Physics, 115*, 8, 3878-3887.

Sokhan, V. P. and N. Quirke (2004). Interfacial friction and collective diffusion in nanopores. *Molecular Simulation, 30*, 4, 217-224.

Song, L. Y., D. Feng, C. G. Campbell, D. Gu, A. M. Forster, K. G. Yager, N. Fredin, H. J. Lee, R. L. Jones, B. D. Vogt and D. Y. Zhao (2010). Robust conductive mesoporous carbon-silica composite films with highly ordered and oriented orthorhombic structures from triblock-copolymer template co-assembly. *Journal of Materials Chemistry, 20*, 9, 1691-1701.

Standeker, S., Z. Novak and Z. Knez (2007). Adsorption of toxic organic compounds from water with hydrophobic silica aerogels. *Journal of Colloid and Interface Science, 310*, 2, 362-368.

Straathof, A. J. (2003). Auxiliary phase guidelines for microbial biotransformations of toxic substrate into toxic product. *Biotechnology Progress, 19*, 3, 755-762.

Tabata, M., I. Adachi, Y. Ishii, H. Kawai, T. Sumiyoshi and H. Yokogawa (2010). Development of transparent silica aerogel over a wide range of densities. *Nuclear*

Instruments & Methods in Physics Research Section a-Accelerators Spectrometers Detectors and Associated Equipment, 623, 1, 339-341.

Trzpit, M., M. Soulard and J. Patarin (2009). Water intrusion in mesoporous silicalite-1: an increase of the stored energy. *Microporous and Mesoporous Materials, 117*, 3, 627-634.

van Deemter, J. J., F. J. Zuiderweg and A. Klinkenberg (1956). Longitudinal Diffusion and Resistance to Mass Transfer as Causes of Nonideality in Chromatography. *Chemical Engineering Science, 5*, 6, 271-289.

Vazquez, G., E. Alvarez and J. M. Navaza (1995). Surface-tension of alcohol plus water from 20-degrees-C to 50-degrees-C. *Journal of Chemical and Engineering Data, 40*, 3, 611-614.

Wagh, P. B., S. V. Ingale and S. C. Gupta (2010). Comparison of hydrophobicity studies of silica aerogels using contact angle measurements with water drop method and adsorbed water content measurements made by Karl Fischer's titration method. *Journal of Sol-Gel Science and Technology, 55*, 1, 73-78.

Walker, G. (1998). Yeast growth. *Yeast: Physiology and Biotechnology*. G. Walker. New York, Wiley**:** 101-202.

Weber, S., C. Briens, F. Berruti, E. Chan and M. Gray (2006). Agglomerate stability in fluidized beds of glass beads and silica sand. *Powder Technology, 165*, 3, 115-127.

Weber, S., C. Briens, F. Berruti, E. Chan and M. Gray (2008). Effect of agglomerate properties on agglomerate stability in fluidized beds. *Chemical Engineering Science, 63*, 17, 4245-4256.

Yomano, L. P., S. W. York and L. O. Ingram (1998). Isolation and characterization of ethanol-tolerant mutants of *Escherichia coli* KO11 for fuel ethanol production. *Journal of Industrial Microbiology & Biotechnology, 20*, 2, 132-138.

Yuan, W. and Y. Sun (2009). Effect of ionic capacity on dynamic adsorption behavior of protein in ion-exchange electrochromatography. *Separation and Purification Technology, 68*, 1, 109-113.

Yuan, W., Y. P. Zhao, Q. Zhang and Y. Sun (2010). Protein adsorption-dependent electro-kinetic pore flow: modeling of ion-exchange electrochromatography with an oscillatory transverse electric field. *Electrophoresis, 31*, 5, 944-951.

Zheng, Y. N., L. Z. Li, M. Xian, Y. J. Ma, J. M. Yang, X. Xu and D. Z. He (2009). Problems with the microbial production of butanol. *Journal of Industrial Microbiology & Biotechnology, 36*, 9, 1127-1138.

Zhuang, X., C. M. Feng, Y. Shen, D. Y. Zhao and Y. Wan (2009). Highly efficient adsorption of bulky dye molecules in wastewater on ordered mesoporous carbons. *Chemistry of Materials, 21*, 4, 706-716.